



# Distinguishing between Apollo 14 impact melt and pristine mare basalt samples by geochemical and textural analyses of olivine

A.L. Fagan<sup>a,b,\*</sup>, C.R. Neal<sup>a,b</sup>, A. Simonetti<sup>a</sup>, P.H. Donohue<sup>a,b</sup>, K.M. O'Sullivan<sup>a,b</sup>

<sup>a</sup> Department of Civil Engineering and Geological Sciences, University of Notre Dame, Notre Dame, IN 46556, United States

<sup>b</sup> NASA Lunar Science Institute, United States

Received 14 April 2012; accepted in revised form 14 December 2012

## Abstract

Apollo 14 (A-14) impact melt olivine vitrophyres (OVs), composed of olivine phenocrysts in an opaque glass matrix with minor amounts of pyroxene and plagioclase, are petrographically similar to pristine quenched A-14 high-alumina (high-Al) and Apollo 12 (A-12) basalts. Textural and chemical analyses have been conducted on olivines within impact melt and pristine mare basalt clasts from A-14 breccia 14321 as well as various olivine-phyric Apollo 12 and 17 basalts to be able to distinguish between the petrographically similar samples. The A-14 high-Al basalts examined here represent samples from each of the three chemical groups (A, B, C). Examples from the three A-12 basalt suites (Ilmenite, Olivine, Pigeonite) and olivine-rich Apollo 17 (A-17) Type C basalt, 74275, have also been analyzed. As a complement to the chemical analyses, crystal size distributions (CSDs) were determined for approximately half of the samples investigated here (due to a small number of olivine crystals that did not produce statistically meaningful CSDs on half of the samples), and confirm that although similar, the basalts and impact melts are texturally distinct. Olivines from A-14 impact melts have the highest average forsterite contents (average Fo  $\sim$ 0.82) and generally the lowest average Co (37 ppm) and Mn (1544 ppm) abundances, thus chemically distinguishing them from the pristine basalts. In addition, chemical compositions obtained for olivine from 14321, 1486 are most likely representative of an impact melt and thus contradict its previous classification as a high-Al basalt (Neal et al., 1988); olivine from, 1486 have similar average forsterite (average Fo  $\sim$ 0.82) and Ti/V-ratio to the OVs. Furthermore, on the basis of their chemical compositions, olivines have been identified within the impact melts that are likely inherited from basalts; these olivines are chemically distinct from the rest of the impact melt olivine population with lower forsterite (0.67–0.80) and low Ti/V ( $\sim$ 10), which are similar to olivine compositions from the A-14 high-Al basalts. In addition to distinguishing between sample types from A-14, olivine compositions can also be used to distinguish between pristine mare basalts from various missions. Olivine within the selected samples from the individual A-12 basalt suites can also be distinguished chemically from one another using the Ti/V ratio, where Olivine suite basalts have Ti/V  $<$ 3 and Ilmenite suite basalts have Ti/V  $>$ 3.5. The results indicate that combined use of CSDs and chemical analyses of olivine can be used to reliably distinguish between (1) impact melts and pristine Apollo 14 basalts, (2) basalts from different landing sites, and (3) individual basalt suites from a single site.

© 2012 Elsevier Ltd. All rights reserved.

## 1. INTRODUCTION

Apollo 14 (A-14) landed in the Fra Mauro region of the Moon ( $-3.7^\circ\text{N}$ ,  $-17.5^\circ\text{E}$ ) and returned  $\sim$ 42 kg of geologic

samples that were predominantly impact-generated breccias. Some of these breccias contained basaltic clasts of an age  $>$ 4 Ga, which is substantially older than mare basalts from earlier missions ( $\leq$ 3.85 Ga; Taylor, 1982) indicating active volcanism in the region at an earlier stage of lunar evolution (Taylor et al., 1983; Dasch et al., 1987). The A-14 basalts, coined “high-alumina” by Ridley (1975), are relatively rich in  $\text{Al}_2\text{O}_3$  (11.1–13.8 wt.%;

\* Corresponding author. Present address: Center for Lunar Science and Exploration, Lunar and Planetary Institute, Houston, Texas 77058, United States.

E-mail address: [fagan@lpi.usra.edu](mailto:fagan@lpi.usra.edu) (A.L. Fagan).

Dickinson et al., 1985) compared to other mare basalts (<8 wt.%, c.f. Lunar Mare Basalt Database – <http://www.nd.edu/~cneal/Lunar-L/>). High-alumina (high-Al) basalts are predominantly composed of pyroxene (50%) and plagioclase (25–40%) with minor olivine (0–10%) and accessory phases (5–15%) such as ilmenite, cristobalite, chromite, whitlockite, glasses and metallic Ni–Fe (Neal et al., 1988, 1989a; Hagerty et al., 2005). In addition, Ti-chromite and Cr-ulvöspinel are present in most basalt clasts from breccia 14321 (Shervais et al., 1985a). These basalts exhibit moderate variation in the abundance of compatible elements (Sc, Cr, Ni, Co, V; Neal et al., 1988, 1989a,b), large ion lithophile elements (K, Rb, Ba, Sr, Cs) and high field strength elements (Zr, Hf, Ta, U, Th; Neal et al., 1989b). Of significance, many of the high-Al basalts contain a KREEP (i.e. composition rich in K, P, and rare-earth elements) signature preserved in their trace element abundances (e.g. Dickinson et al., 1985; Shervais et al., 1985a; Neal et al., 1989a,b; Neal and Kramer, 2006), and appear to have been crystallized in three distinct episodes at ~4.3, ~4.1, and ~3.9 Ga (Papanastassiou and Wasserburg, 1971; Compston et al., 1971, 1972; Mark et al., 1973, 1975; Taylor et al., 1983; Dasch et al., 1987, 1991). This KREEP component may have been added by (1) assimilation with a primitive high-Al basaltic magma (Neal et al., 1988), (2) mixing of KREEP-rich crustal materials along with mare basalts and ferroan anorthosites via impact melting (Hagerty et al., 2005), or (3) incorporation of low melting point components as the high-Al magmas flowed across the lunar surface (Hui et al., 2011).

An apparent discord between Sm–Nd and Rb–Sr ages for the high-Al basalts has led some authors to suggest an impact origin for all basaltic clasts found in A-14 breccias (Snyder et al., 2000; Snyder and Taylor, 2001). For example, Dasch et al. (1987) reported both Rb–Sr and Sm–Nd ages for several high-Al basalt clasts from breccia 14321; they noted that the Rb–Sr ages ( $4.12 \pm 0.15$  Ga) were older than the Sm–Nd ages ( $3.75 \pm 0.35$  Ga), although these are essentially indistinguishable given the uncertainty associated with the latter. Errors were magnified by the relatively poor precision on each Sm–Nd determination, as well as the small spread in Sm/Nd ratios for the different splits used to construct the isochrons (Dasch et al., 1987). Snyder and Taylor (2001) suggested that the Sm–Nd systematics of the majority of the high-Al basalts were disturbed and that the Rb–Sr ages may not represent true crystallization ages. Rather, they may represent a weighted average of the total Sr budget for the target rocks that were mixed during the meteorite impact, which would represent a two-component mixture of a ferroan-anorthosite (FAN) and KREEP (Snyder et al., 2000). While Ridley (1975) and Warren et al. (1997) argued that the A-14 high-Al basalts were pristine, internally derived lunar melts, Snyder and Taylor (2001) noted that the absence of elevated Ir contents does not discount an impact origin.

Hagerty et al. (2001, 2002, 2003, 2005) conducted a secondary ion mass spectrometry (SIMS) study of olivine and plagioclase grains in the high-Al basalts, and demonstrated that these reflect the whole rock basalt compositions; hence concluding that the observed spread in the whole rock data

is not the result of short-range unmixing (Haskin et al., 1977; Lindstrom and Haskin, 1978). On the basis of Ni contents for olivine, Hagerty et al. (2001, 2002, 2003, 2005) argued that these phenocrysts represent early-forming crystals in a pristine fractionating magma. The low non-volatile to volatile ratios (e.g., Ba/Rb) of the melt supports the contention that the high-Al basalts are pristine mare basalts (Hagerty et al., 2003), but Hagerty et al. (2005) noted that an impact origin could not be completely ruled out. Neal and Kramer (2006) compared the major and trace element compositions of olivine phenocrysts in these basalts with those in known impact melts and concluded that the A-14 high-Al basalts are pristine.

A second group of important clasts found in the A-14 breccias, impact melt-olivine vitrophyres (e.g. Allen et al., 1979; Shervais et al., 1988) are composed primarily of olivine phenocrysts in an opaque glass matrix with occasional pyroxenes and lath-like plagioclase crystals. Although petrographically similar to quenched high-Al basalts and some Apollo 12 (A-12) basalts, these impact melt olivine vitrophyres (OVs) are distinguished by high modal olivine, high siderophile element abundances such as Ni and Ir, high MgO, and low CaO/Al<sub>2</sub>O<sub>3</sub> ratios (Shervais et al., 1988); additionally, olivine in the OVs have higher forsterite (Mg/Mg + Fe) values (Fo, 0.67–0.88) than in the high-Al basalts (Fo, 0.50–0.76; Neal and Kramer, 2006). The high MgO content, typically indicative of a primitive magma, is in contrast with elevated abundances of incompatible trace elements, which generally indicate a more evolved magma (Neal and Taylor, 1988). This dichotomy between major and trace element chemistry was addressed by formation through meteorite impact mixing (Allen et al., 1979). Shervais et al. (1988) described a mixing process involving an impact melt composed of KREEP, granite, ferroan anorthosite, meteoritic material (CI chondrite; Boynton et al., 1975), alkali suite anorthosite and a “high-Mg” component. Neal and Taylor (1989) modified this mixing behavior by separating the KREEP component through liquid immiscibility into a K-fraction (granite, 14–16%) and a REEP-fraction (phosphate, ilmenite, fayalite, 0.1–1.8%) along with highlands (troctolite and dunite, 51–58%), mare basalt, (A-14 high-Al basalt, 25–30%) and meteoritic (1.7–2.5%) components. By splitting the KREEP into K- and REEP-fractions, the model described by Neal and Taylor (1989) reduced the overall quantity of the KREEP component required to generate the trace elements observed in the OVs, thus eliminating the need to infer a hypothetical “high-Mg” component.

Although whole-rock highly siderophile element analyses can be used to distinguish between the petrographically similar A-14 high-Al basalts and OVs, these methods are time-consuming, destructive, and require a substantial amount of limited (and precious) sample material. It is important to be able to distinguish between these samples, as different scientific objectives require the use of one sample type or the other. For example, a study of the bombardment history of the Moon requires the use of impact melt samples while a study of the thermal history of the lunar interior would find basalt samples far more useful. Thus, it is imperative to be able to distinguish between these precious samples in a timely

and minimally destructive manner. The objective of this paper is to distinguish between the A-14 impact melt OV and pristine mare basalts using olivine mineral chemistry and petrographic evidence. A combined textural and chemical analytical approach is used to examine impact melt and pristine mare basalt samples to provide information about the melts from which the minerals crystallized.

## 2. SAMPLES

Petrographic thin-sections from 13 impact melt and high-Al basalt clasts (Table 1; Fig. 1) were analyzed from the A-14 breccia 14321 (e.g. Duncan et al., 1975); each clast has been previously analyzed for both major element mineral and whole rock chemistries, with the exception of subsample 14321,1486, which was too small (parent mass < 0.05 g) for whole rock analysis (Table 2). The high-Al basalts represent samples from each of the three groups (Table 1; A, B, C) proposed by Neal and Kramer (2006) that cover a wide range of incompatible element abundances and ratios. Additionally, 10 A-12 pristine mare basalts and one olivine-rich Apollo 17 (A-17) basalt were also examined (Table 1; Fig. 1).

A-14 OVs contain abundant olivine microphenocrysts, set in a devitrified glass matrix, with textures indicating quenching from above or near liquidus temperatures (e.g. Allen et al., 1979). These samples display predominantly euhedral olivine crystals (0.05–0.4 mm) with occasional subhedral to anhedral olivine grains (0.1–0.5 mm). Some olivine crystals contain small glass inclusions (<0.05 mm)

while chromite inclusions (<0.05 mm) are only found in the largest phenocrysts. Plagioclase laths (<0.5 mm in length) are also present in subsamples ,1305 and ,1486. Of note, we classify ,1486 as an impact melt, though it is not an OV (see below).

The A-14 high-Al basalts (Table 1) in this study are dominantly holocrystalline with intersertal (e.g. ,1246; Fig. 1) to subophitic (e.g. ,1480; Fig. 1) textures. Group B and C basalts are comprised of euhedral to subhedral olivine (0.1–1.9 mm), pyroxene, and plagioclase crystals. In contrast, Group A basalts may contain only minor pyroxene (,1246; Fig. 1) or minor olivine (,1611; Fig. 1); when present, most olivine from Group A basalts are 0.1–0.5 mm with the exception of the 1.5 mm olivine from 14321,1246 (Fig. 1). Group C basalts also contain well-developed plagioclase laths up to 1.5 mm in length. These basalts may contain olivine with melt or chromite inclusions.

A-12 Olivine suite basalts (12004; 12015; 12020; Fig. 1) are composed predominantly of olivine and pyroxene in a variolitic groundmass of clinopyroxene and plagioclase (Brett et al., 1971; Klein et al., 1971; French et al., 1972; Papike et al., 1976; Neal et al., 1994a); the olivine in some thin-sections of this suite display a glomerophyric texture (12020; Fig. 1). Olivine crystals in these basalts are predominantly euhedral to subhedral (0.3–0.9 mm) set amongst elongate pyroxenes up to 2.5 mm in length. Chromite inclusions can be found in some olivine grains. Sample 12015 (Fig. 1) differs from the other members of this suite with its vitrophyric texture. Although it may appear to be

Table 1  
Sample types and analyses performed.

Thin section #	Sample type <sup>a</sup>	Olivine chemistry	Textural analysis
14321			
,1246	A-14 Group A basalt	✓	NP
,1305	A-14 OV-IM	✓	✓
,1376	A-14 Group B basalt	✓	NP
,1471	A-14 OV-IM	✓	✓
,1480	A-14 Group A basalt	✓	NP
,1482	A-14 Group B basalt	✓	NP
,1483	A-14 Group B basalt	✓	NP
,1486	A-14IM	✓	✓
,1602	A-14 OV-IM	✓	✓
,1611	A-14 Group A basalt	✓	NP
,1612	A-14 Group B basalt	✓	NP
,9057	A-14 Group C basalt	✓	NP
,9080	A-14 Group C basalt	✓	NP
12004,137	A-12 Olivine basalt	✓	✓
12005,44	A-12 Ilmenite basalt	✓	NP
12008,65	A-12 Vitrophyric Ilmenite basalt	✓	✓
12015,29	A-12 Vitrophyric Olivine basalt	✓	✓
12016,41	A-12 Ilmenite basalt	✓	✓
12019,5	A-12 Pigeonite basalt	✓	NP
12020,14	A-12 Olivine basalt	✓	✓
12020,57	A-12 Olivine basalt	✓	✓
12052,345	A-12 Pigeonite basalt	✓	NP
12065,109	A-12 Pigeonite basalt	✓	NP
74275,312	A-17 Type C basalt	✓	✓

<sup>a</sup> A, B, and C basalt groups classified by Neal and Kramer (2006); IM defined as impact melt; OV-IM defined as impact melt olivine vitrophyre; NP signifies samples where textural analysis was not possible; A-17 'C' basalt categorized by Rhodes et al. (1976).

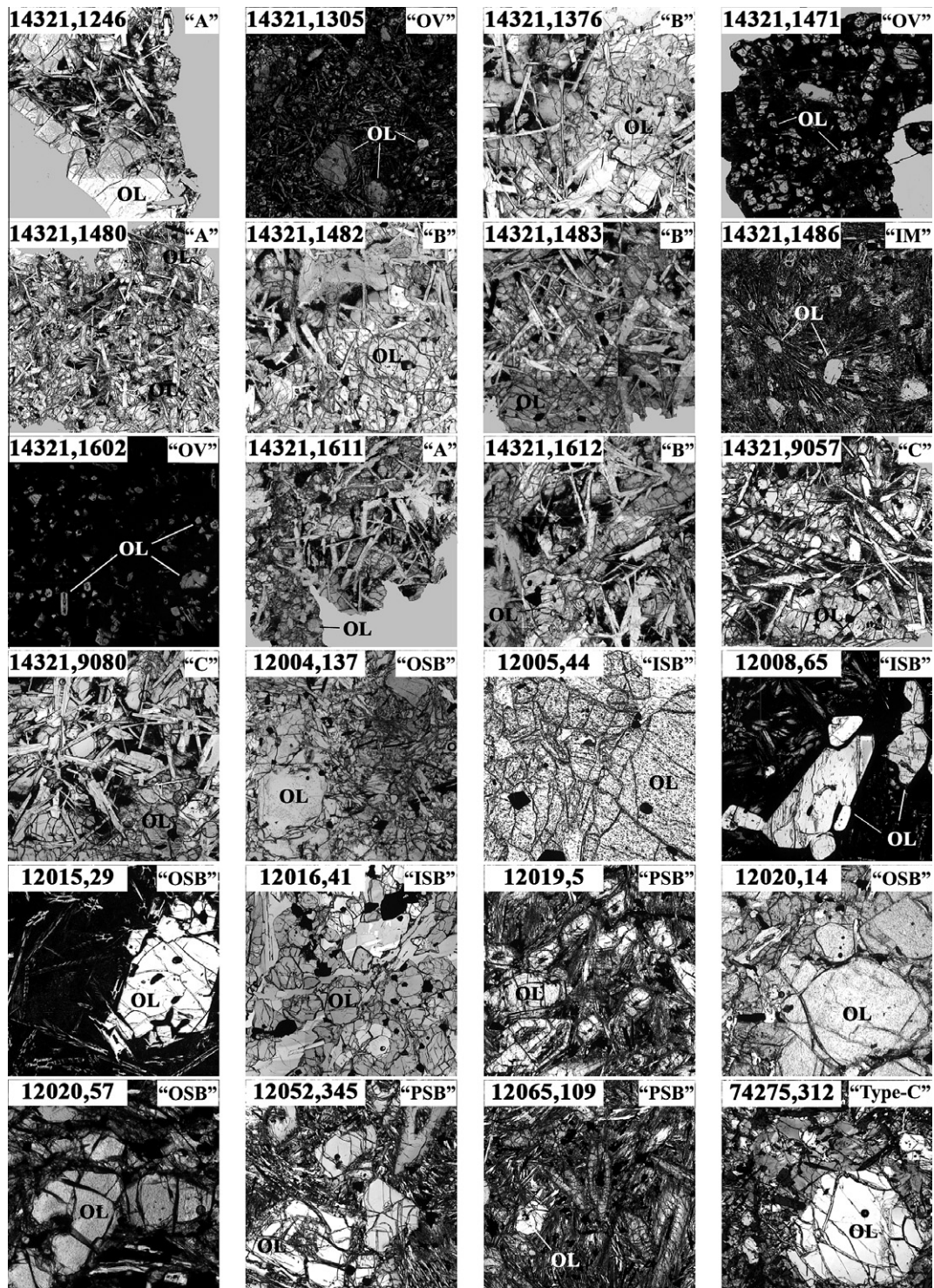


Fig. 1. Representative plane-polarized light photomicrographs of each sample examined in this study. Each sample image is 1 mm  $\times$  1 mm in dimension. Sample types can be found in Table 1. Abbreviations stand for the following: OV is olivine vitrophyre impact melt; “A”, “B”, and “C” are A-14 basalt types; IM is impact melt (not an OV); ISB, OSB, and PSB are A-12 Ilmenite, Olivine, and Pigeonite suite basalts, respectively. Olivine crystals are identified in each sample by “OL”.

texturally similar to the A-14 OVs, 12015 is a pristine mare basalt rather than an impact melt (e.g. Snyder et al., 1997). Sample 12015 displays quenched textures with

euhedral to subhedral olivine (0.1–1.0 mm), skeletal olivine (0.2–1.2 mm), and skeletal pyroxene (0.15–1.10 mm).

Table 2  
Sources for whole-rock data in Fig. 2.

Sample #	Whole rock source
14321	
,1246	Shervais et al. (1984)
,1305	Shervais et al. (1988)
,1376	Neal et al. (1988)
,1471	Neal and Taylor (1989)
,1480	Neal et al. (1988)
,1482	Neal et al. (1989b)
,1483	Neal et al. (1989b)
,1486	No Whole Rock data available
,1602	Neal and Taylor (1989)
,1611	Neal et al. (1989b)
,1612	Neal et al. (1989b)
,9057	Dickinson et al. (1985)
,9080	Dickinson et al. (1985)
12004	Wakita et al. (1971)
12005	Rhodes et al. (1977) and Nyquist et al. (1977)
12008	Neal (2001)
12015	Neal (2001)
12016	Neal et al. (1994a,b)
12019	Neal et al. (1994a,b)
12020	Wakita et al. (1971)
12052	Wänke et al. (1971) and Schnetzler and Philpotts (1971)
12065	Maxwell (1971)
74275	Rhodes et al. (1976) and Wänke et al. (1974)

Three samples have been examined from the A-12 Ilmenite suite: 12005, 12016, and 12008 (Fig. 1; Table 1). Although 12005 is classified as an Ilmenite suite basalt, it contains relatively minor ilmenite ~2% (Rhodes et al., 1977; Neal et al., 1994a) and texturally appears to have accumulated olivine. It contains large zoned olivine grains (up to 1 mm) and zoned pyroxene phenocrysts (up to 1 mm) that may enclose olivine, set in a groundmass of olivine, pyroxene, plagioclase, and ilmenite (Fig. 1). Zoned pyroxene phenocrysts contain augite cores and pigeonite rims. In contrast, sample 12016 is equigranular (Dungan and Brown, 1977) with pyroxene (0.2–0.8 mm), ilmenite (0.05–0.34 mm), and 12% un-zoned olivine (Neal et al., 1994a) ranging 0.05–0.8 mm in size (Fig. 1); sample 12016 contains ~5% ilmenite (Dungan and Brown, 1977; Neal et al., 1994a). Pyroxenes appear as complex intergrowths of augite and pigeonite with no apparent common zonation pattern. The mesostasis consists of olivine, silica, glass, and phosphate. One sample from the Ilmenite suite in this study has a vitrophyric texture (12008; Fig. 1). Crystal sizes within 12008 are similar to 12015, the vitrophyric Olivine suite basalt. Groundmass in 12008 is variolitic with pyroxene needles radiating from olivine phenocrysts. The morphology of skeletal olivine microphenocrysts within 12008 suggests that they are products of a chain-like second-generation (Donaldson, 1976) that precede the pyroxenes in the crystallization sequence (Dungan and Brown, 1977).

A-12 Pigeonite suite basalts (12019; 12052; 12065; Fig. 1) have similar textures to each other with pyroxene phenocrysts dominating the fine-grained groundmass and relatively few olivine phenocrysts (~0.2–0.8 mm). The three

basalts exhibit variolitic groundmass with needles of pyroxene and plagioclase radiating from phenocrysts. Pyroxene phenocrysts (0.2–>2 mm) may display an intra-fasciculate texture, with hollow cores forming in the middle of pyroxene phenocrysts are later filled with a microcrystalline assemblage of pyroxene, plagioclase, ilmenite, and metal (Drever et al., 1972). This texture along with the variolitic texture of the groundmass is usually associated with rapid crystallization (Drever et al., 1972).

A-17 sample 74275,312 (Fig. 1) is an olivine porphyritic (texturally Type IA after Brown et al., 1975; chemically Type C after Rhodes et al., 1976), high-titanium basalt (e.g. Papike et al., 1976). It contains phenocrysts of olivine (0.1–1.2 mm), ilmenite (0.2–1 mm in length), pyroxene (up to 0.5 mm), and plagioclase laths (0.2–1 mm). Olivine phenocrysts generally contain small, euhedral chromite inclusions and occasionally exhibit pyroxene reaction rims (~30–85  $\mu$ m). One olivine phenocryst (0.7 mm) appears hollow, although this may represent plucking during the thin section polishing procedure. Armalcolite forms cores to, or is partly mantled by, ilmenite. The subvariolitic- to plumose-textured groundmass is dominated by clinopyroxene, plagioclase, and ilmenite, with minor Fe-metal and silica.

### 3. ANALYTICAL PROCEDURES

#### 3.1. Mineral chemistry analysis

Major element analyses were performed via electron-probe microanalysis (EPMA) using a JEOL JXA-8200 electron microprobe at the Earth and Planetary Sciences Microanalysis Facility housed at Washington University in St. Louis. All crystals were analyzed using a 15 kV accelerating potential, 25 nA beam current, 5  $\mu$ m spot size, and 30 s on-peak counting time. Natural and synthetic mineral standards were used for both the primary calibration and secondary checks of that calibration including Kakanui hornblende as a long term stability standard. Detection limits for individual elements are 0.01–0.03 wt.%. Data were reduced using *Probe for Windows* software and are reported with stoichiometry in Table EA1 within the Electronic Annex.

Trace elements (Ca, Sc, Ti, V, Cr, Mn, Co, Ni, and Y) were quantified by laser ablation-inductively coupled plasma-mass spectrometry (LA-ICP-MS) over the course of ten individual sessions; early sessions did not quantify Ca and the setup was changed to better characterize the olivine thereafter. The analytical protocol involved the use of a New Wave UP-213 laser ablation system with He carrier gas coupled with a Thermo-Finnigan Element2 ICP-MS instrument at the University of Notre Dame's Midwest Isotope and Trace Element Research Analytical Center (MITERAC). Mn abundances obtained by EPMA were used as the internal standard, while the NIST SRM 610 glass was employed as the external standard. The NIST SRM 610 glass standard was selected because its Mn abundance (~458 ppm; Pearce et al., 1997) is similar to those measured for the olivines investigated here. LA-ICP-MS analyses were conducted using a repetition rate of 5 Hz,

spot diameter of 15–25  $\mu\text{m}$  (dependent on size of olivine crystals) and corresponding fluence of  $\sim 17 \text{ J/cm}^2$ . Measurements of the NIST SRM 610 glass were taken at the beginning and end of each analysis set. Deviation to the accepted NIST SRM 610 values (e.g. Pearce et al., 1997) are within the error determined by Jochum et al. (2011) for LA-ICP-MS using a 25  $\mu\text{m}$  spot size. For each analysis, the laser was allowed to warm-up for  $\sim 20 \text{ s}$ , take background counts for 30 s, and then ablate the sample for 1 min. After  $\sim 45 \text{ s}$ , this process was repeated for the next analysis. Elemental abundances were determined using *GLITTER*© software (XP version, Simon Jackson, Macquarie University) and are reported, with their associated errors, in Table EA2 within the Electronic Annex. Of note, detection limits for Ni vary significantly from 3 ppm to well over 500 ppm, which is due to the introduction of a new cone to the ICP-MS system; this dramatically heightened the sensitivity of the instrument and thereby reduced the detection limit for Ni to as little as 3 ppm.

### 3.2. Textural analysis

Crystal size distributions (CSDs) can be used as a complement to compositional analyses and to quantitatively investigate igneous processes, such as the residence time of the crystal population as a function of the CSD slope (e.g., Cashman and Marsh, 1988; Higgins, 1996). Here, we use the overall slope of the CSD from different samples to distinguish between their crystallization histories as further confirmation of the distinction between basaltic and impact melt samples. Olivine CSDs were determined for three A-14 OVs, four A-12 Olivine suite basalts, two A-12 Ilmenite suite basalts, one Type C A-17 basalt, and one sample (14321,1486) which was previously classified as a basalt (Neal et al., 1988), but we reclassify as an impact melt (Table 1). These samples were selected for CSD analysis based on their relatively olivine-rich textures (i.e.  $>100$  crystals), allowing CSD analysis. No CSD analyses were performed on the A-14 high-Al basalts because these samples had  $<100$  olivine crystals, which produced CSDs with large errors, making them not statistically meaningful. For CSD analyses, individual olivine crystals were traced over thin-section mosaics (plane- and cross-polarized light) created from digital photomicrographs using *Adobe Photoshop*®. The resulting crystal layers were imported into *ImageJ* (Higgins and Chandrasekharam, 2007), which measures the major and minor axes, roundness, and area of each crystal. *ImageJ* is used in preference over the older *ImageTool* (Higgins, 2000) because *ImageJ* can accommodate larger image file sizes, thus better retaining the integrity of the smallest crystals. Individual crystals with minor axes  $<0.03 \text{ mm}$  were not included in final CSD analyses, as these dimensions are more likely to be a projection of a crystal rather than an accurate measurement due to the approximately equivalent thickness of the thin-section (Higgins, 2000). The major and minor axes of crystals  $\geq 0.03 \text{ mm}$  were imported into *CSD-slice* (Morgan and Jerram, 2006) to determine the best-fit short, intermediate, and long axes of the 3D crystal habit. These data, in conjunction with the major and minor axes, individual crystal area, average crystal roundness, and total

sample area, were used in *CSDcorrections 1.39* (Higgins, 2000; Higgins and Chandrasekharam, 2007) to determine the 3D CSD using 5 bins per decade. Analytical uncertainties were also calculated by *CSDcorrections* and represent the minimum and maximum of the square-root of the number of intersections of crystals with a plane per bin (Higgins, 2000). Finally, CSDs are plotted as the natural log of the population density against the corrected crystal size length (Cashman and Marsh, 1988). Crystallization under steady-state conditions is reflected by linear CSDs on this semi-logarithmic plot.

## 4. RESULTS

### 4.1. Whole rock chemistry

Whole rock rare earth element (REE) abundances can be used to distinguish between the OVs and the basalt groups from the various Apollo sites (Fig. 2; data sources in Table 2). The A-14 OVs have the highest REE abundances among the sample set followed by A-14 Groups B, C, and A respectively (Fig. 2a). The A-12 basalts have intermediate compositions between the A-14 Group C and A basalts. Amongst the A-12 basalts, the Pigeonite suite basalts have the highest REE abundances followed by the Olivine and Ilmenite suite basalts, respectively (Fig. 2b). Sample 12015 (vitrophyric Olivine suite basalt) is indistinguishable from other members of its suite with respect to whole rock data. In contrast, the vitrophyric Ilmenite suite basalt, 12008, has REE abundances similar to a Pigeonite suite basalt rather than that of an Ilmenite suite basalt. A-17 sample 74275 is Light-REE depleted ( $\text{La}/\text{Sm}_N = 0.4$ ), which is in stark contrast to the basaltic REE patterns from A-12 ( $\text{La}/\text{Sm}_N = 0.7\text{--}0.9$ ) and A-14 ( $\text{La}/\text{Sm}_N = 0.9\text{--}1.3$ ) as well as those from the A-14 OVs ( $\text{La}/\text{Sm}_N = 1.5$ ).

### 4.2. Olivine chemistry

Distinct chemical differences exist between olivines in the A-14 OVs (and 14321,1486 impact melt) and the mare basalts from A-12, A-14, and A-17 (Tables EA1 and EA2). In particular, the olivine in A-14 OVs have the highest forsterite values (Fo, 0.67–0.88, Fig. 3a; Table EA1) in comparison to those from the A-14 high-Al basalts (Fo, 0.50–0.76) and A-12 basalt suites (Fo, 0.58–0.78). A-17 basalt 74275,312 contains olivine with intermediate Fo-values (0.74–0.82) to the A-14 OVs and the mare basalts from both A-12 and A-14. In addition to lower Mg abundances (i.e. lower Fo), olivine in the selected A-14 and A-12 pristine mare basalts typically have higher average Co (Fig. 3a; A-14: 49–75 ppm; A-12: 90–117 ppm) and Mn (Fig. 4; A-14: 2318–2889 ppm; A-12: 1997–2824 ppm) abundances than those in the OVs (Co: 22–40 ppm; Mn: 1474–1515 ppm). Olivine crystals from these pristine basalts typically have lower average abundances of the incompatible trace element Y, particularly those from A-12 (Fig. 4a; Table EA2). Furthermore, the A-12 basalts with vitrophyric textures (12008; 12015) contain olivine grains with the highest average abundances of Co (113–117 ppm; Fig. 3a) and Sc (10–11 ppm; Fig. 4b) among the samples investigated here

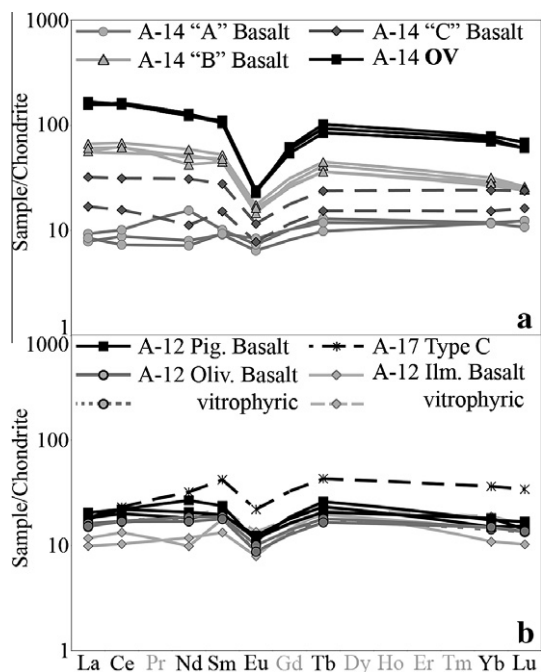


Fig. 2. Chondrite-normalized (Taylor and McLennan, 1985) whole-rock REE abundances: (a) A-14 basalt groups and impact melts as defined by Neal and Kramer (2006) and (b) A-12 basalt suites and A-17 'C' basalt, 74275. Whole-rock data obtained by sources listed in Table 2. Data for REE in grey are interpolated.

(Table EA2). Olivine from 14321,1486 are chemically similar to the A-14 OVs, though at least two rounded and embayed crystals are compositionally similar to the A-14 high-Al basalts or 74275 (Figs. 3–5). Additionally, one rounded olivine from A-14 OV 14321,1602 is also chemically similar to the A-14 high-Al basalts rather than the OVs (Figs. 3–5).

The olivine from the A-12 basalts with vitrophyric textures (12008; 12015) can be distinguished from those in the other basalt suites based on their Sc abundance or Ti/V ratio (Fig. 6). A-12 Olivine suite basalts contain olivine with the lowest Ti/V ratio (<3), but those from 12015 have distinct Sc abundances (<15 ppm) from the rest of the suite (12004 & 12020); olivine from 12004 and 12020 have the highest Sc abundances (>18 ppm) of all basaltic olivine examined here. Conversely, while olivine from vitrophyric Ilmenite suite basalt, 12008, have similar Sc abundances (8.8–13.3 ppm) to the rest of the suite, they typically display a low Ti/V ratio (3.7–4.8) in comparison to 12005 and 12016 (4.5–12.2) (Fig. 6). Olivine crystals from the Pigeonite suite basalts compositionally overlap those from the Ilmenite and Olivine suites basalt (Sc: 8.9–11.5 ppm; Ti/V:1.8–10); there are no trace element data that distinguish the Pigeonite suite basalts from other basalt suites (Table EA2).

Olivine variations are also documented within the A-17 Type C basalt. The smallest crystals in 74275,312 exhibit the lowest Fo (0.74–0.75) and the highest Mn (2038–2201 ppm) and Ti/V (19–28) values within the sample (Tables EA1 and EA2). This likely reflects changes in the

melt composition due to earlier olivine crystallization, but prior to ilmenite or armalcolite becoming liquidus phases.

### 4.3. Textural analyses – crystal size distributions (CSDs)

The majority of the olivine CSD profiles are linear to sub-linear with the OV CSD slopes generally steeper than the A-17 and A-12 basalts (Figs. 7 and 8). However, there are a few exceptions. OV sample 14321,1602 has a slight upward kink at ~0.3 mm likely due to more crystals at the largest size interval than expected by the *CSDslice* model; at least one of these crystals may be inherited as it is chemically similar to A-14 high-Al basalts and represents a distinct crystallization history within the sample (Figs. 3–5). Several samples (12015,29; 12020,14 and,57) have marked downward curves at the smallest crystal size bins (Fig. 8). Finally, three samples (12008, 12015, 74275) display a slightly sinuous CSD profile (Fig. 8), which may in part reflect multiple crystal populations observed in the thin-section. As previously stated, no olivine CSD analyses were performed for A-14 high-Al basalts due to the small number of olivine crystals present. Of note, the CSD of 14321,1486 is similar to those of the OVs and the CSD for 74275,312 appears to have a slope intermediate to the A-14 OVs and the pristine A-12 mare basalts.

## 5. DISCUSSION

### 5.1. Whole-rock vs. mineral chemistry

Whole rock trace element data appears to effectively distinguish impact melts from pristine mare basalts (Fig. 2), but the method is not feasible for small samples (e.g. 14321,1486). Thus, a more universal protocol is the one adopted here of characterizing the major and trace element chemistry of olivine phenocrysts. This method is significantly less destructive, and requires a smaller sample aliquot than that used for the quantification of highly siderophile elements (~2 g), leaving significant portions of sample available for future study.

High forsterite values in olivine have been shown to be characteristic of impact melts (e.g. Shervais et al., 1985b), though recent work has shown that olivine from Mg-suite sample 76535 has an average Fo = 0.88 (Elardo et al., 2012) and olivine from other rock types, such as troctolite, can have Fo-values as high as 0.90 (Shearer and Papike, 2005). The olivine in this study continues the trend of impact melt samples with high Fo. Sample 14321,1486, though not an OV, contains olivine crystals with similarly high Fo. In addition to major element differences, the olivine basalts and impact melts have distinct trace element characteristics. The OVs typically have lower Co than the A-14 high-Al basalts and the A-12 basalts. As Co is highly compatible in olivine (e.g.  $K_D \sim 4.3$ ; Klöck and Palme, 1988), this indicates that the target rock for the OVs, is likely to have had a lower Co composition than reflected in the A-12 and A-14 basalts. Though, recall that at least one olivine from ,1602 is, seemingly paradoxically, similar in composition to the A-14 basalts rather than the OVs

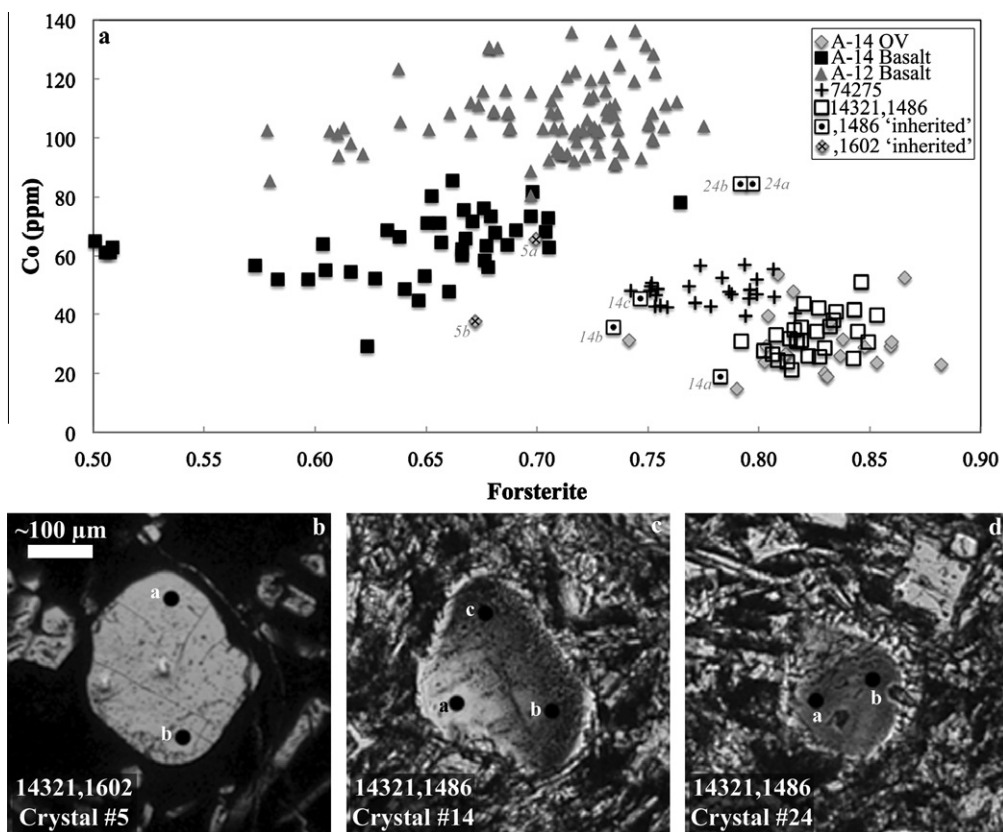


Fig. 3. Co vs. Fo values for olivine crystals in this study by sample type. Analyses of three potentially inherited olivine crystals discussed in the text are labeled in (a) and their plane-polarized light photomicrographs shown in (b–d) with black points indicating the location of each analysis; the size of the black points are not representative of the laser ablation size.

(Figs. 3 and 4). Furthermore, if the target material for the OVs was unlike the A-14 high-Al basalts, the OVs must have interacted with a high-Al composition shortly after impact in order to have at least one unique olivine with similar composition. A-17 sample 74275 contains olivines similar to the OVs in Fo, Co, and Ti/V (Figs. 3 and 5) suggesting that the OV target material may have been a similar composition to 74275, though 74275 olivines are generally less abundant in Y than the OVs (Fig. 4a).

As shown in Fig. 5, the Ti/V ratio for basaltic olivine has an inverse relationship to Fo, with the ratio increasing with later crystallization (i.e. lower Fo). This is more clearly seen in olivines from the A-12 and A-14 basalts than those in 74275, largely because the latter cover a limited range of Fo values, so the data points are more compressed (Fig. 5). In contrast, the olivines from the OVs and ,1486 do not have a readily discernible relationship between the Ti/V ratio and the Fo content. The olivines from the OVs and ,1486 have a larger range of Ti abundance and a limited variation in V in contrast to the basaltic olivines (Fig. 9). Basaltic olivines show a steady increase in Ti with decreasing Fo while those from the OVs and ,1486 show no such relationship (Fig. 9a). Basaltic olivines also display a steadily decreasing V content with Fo while those from the OVs and ,1486 do not (Fig. 9b). In lunar basalts, V is compatible in olivine ( $K_D \sim 1.3$ ; Ringwood, 1970), which

accounts for the decrease in V abundance with later crystallizing olivine within the basalts, as less V is available; this does not explain the behavior of V within the OVs and ,1486. Ti is incompatible in olivine (e.g.  $K_D \sim 0.019$ ; Klöck and Palme, 1988), so later crystals would have higher abundances to reflect the melt becoming increasingly richer in Ti as olivine crystallizes, which is shown in the basalts, but not the OVs and ,1486. It is unclear as to why the impact melt samples behave so dramatically differently than the basaltic samples, although we conclude such behavior is a result of the initial melt composition (i.e. target material) and a non-equilibrium (i.e. quench) crystallization regime.

## 5.2. Sample 14321,1486

Based on petrographic examination, Neal et al. (1988) identified subsample ,1486 as a mare basalt, but this detailed study indicates that it is likely to be an impact melt. The euhedral olivine crystals are similar in composition to those from the OVs (e.g. Figs. 3 and 5), which are impact melts. Low Co abundance (avg.  $\sim 37$  ppm) is characteristic of olivines from 14321 OV clasts, and olivines from subsample ,1486 share this characteristic; this is consistent with ,1486 being an impact melt rather than a pristine mare basalt (Fig. 3; Table EA2), though it does not have a vitrophyric texture. Textural analyses also corroborate this

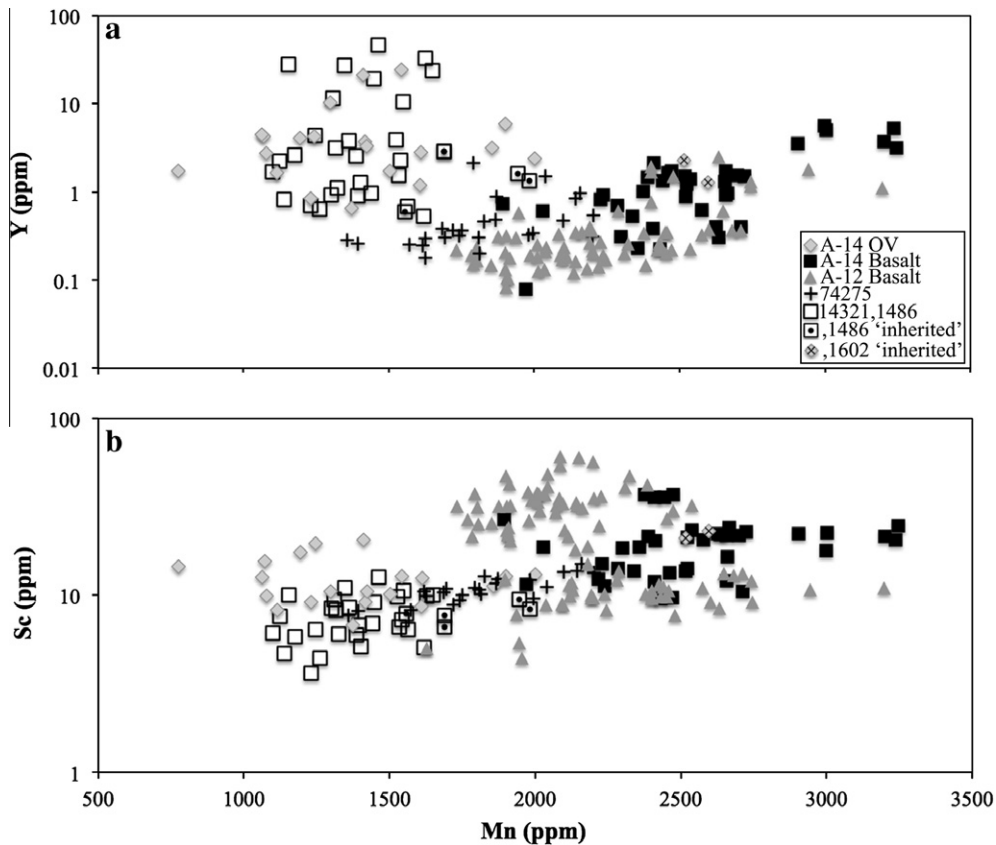


Fig. 4. Mn, Y, and Sc values for olivine crystals in this study separated by sample type. Rounded and embayed crystals from Fig. 3b–d are also identified here by the same symbols as Fig. 3a. See text for discussion.

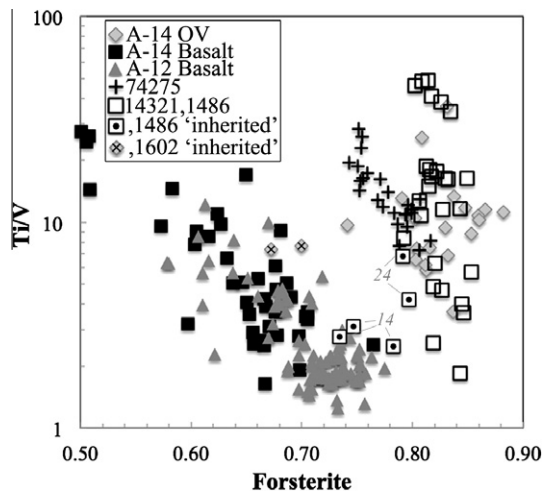


Fig. 5. Ti/V vs. Fo data for the olivine crystals in this study separated by sample type. Potentially inherited crystals discussed in the text are identified by unique symbols.

interpretation; the slope of the ,1486 olivine CSD is similar to the rest of the A-14 impact melts, whereas the slopes of the pristine basaltic CSDs (A-12 & A-17) are shallower indicating a difference in cooling histories between the sample types (Fig. 7).

The chemistry and morphology of euhedral olivines in A-14 impact melts (OVs and ,1486) are reasonably distinct from those in basaltic olivines (Figs. 3–5). The olivines from A-14 impact melts have high Ti-values (Fig. 9; Table EA2), suggesting a similarly elevated level of Ti in the target rock. However, as shown in Fig. 3, three individual olivine grains from the impact melt samples have similar trace element data to olivine from A-14 high-Al basalts or A-17 basalt. Two of these rounded and embayed crystals are found in sample 14321,1486 (Fig. 3c and d), while the third is from 14321,1602 (Fig. 3b). These crystals are likely to be inherited from the target material or interaction with some other surface lithology during crystallization from the impact melt given their distinct shape and chemistry. The relatively low Fo (0.73–0.80) of these rounded crystals suggest that they did not crystallize directly from the impact-induced melt, but rather were inherited from a basalt such as a high-Al A-14 or a basalt similar in composition to 74275 (e.g. Fig. 3a) depending on the crystal. Crystal #14 (,1486; Fig. 3c) is the only relict grain to display compositional zoning visible in both plane- and cross-polarized light as a gradation from light to dark portions (left-to-right in Fig. 3c). Major and trace element variations suggest that the majority of the crystal was inherited (darker region) with a later overgrowth (lighter region) reflecting the crystallization of the impact melt; the darker region may also show evidence of shock in both its distinctive color and

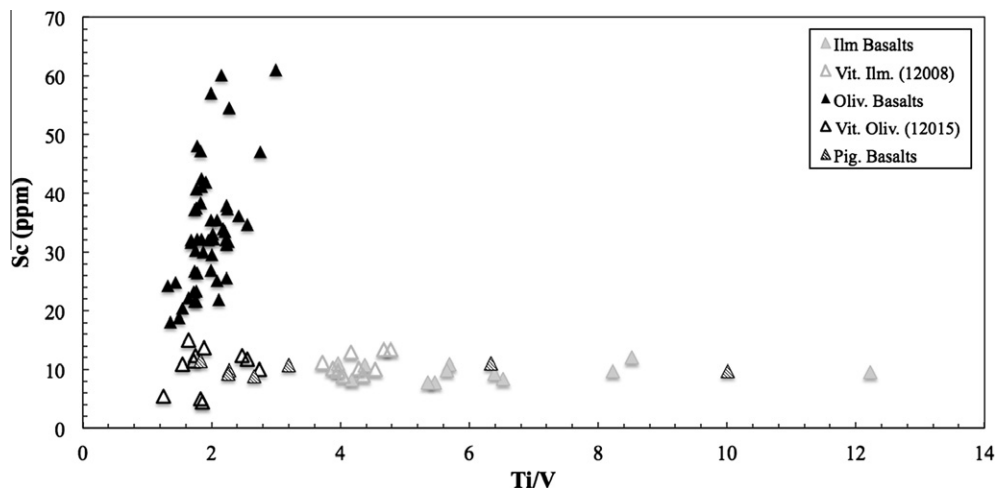


Fig. 6. Sc vs. Ti/V for olivine from the A-12 basalt suites; samples with vitrophyric textures are distinguished from the other members of their respective suite by open symbols.

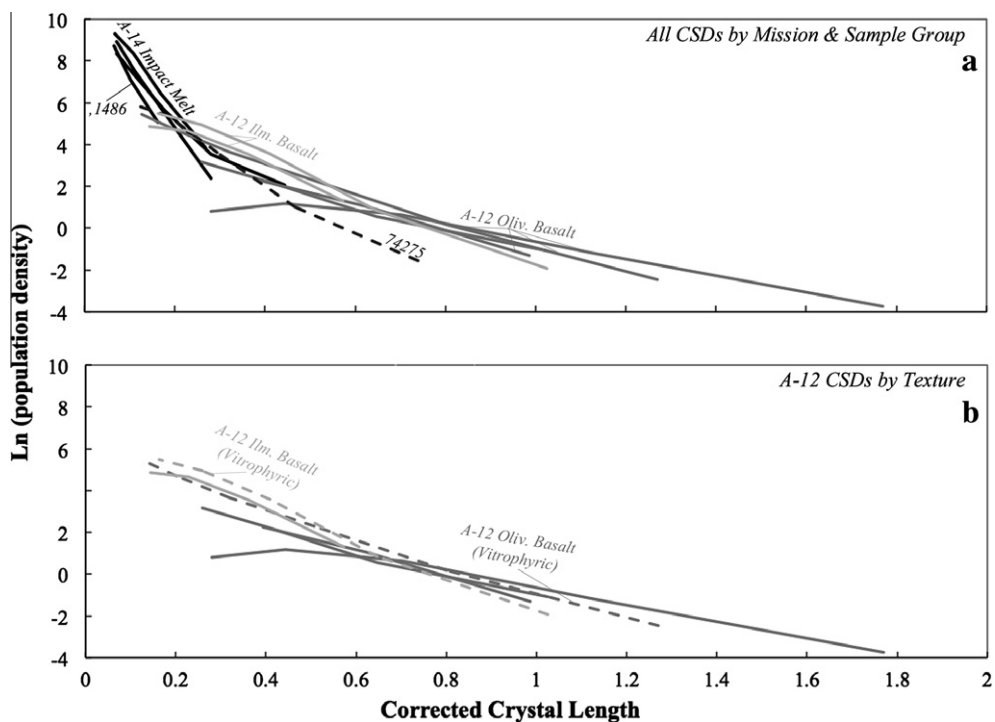


Fig. 7. (a) Semi-logarithmic olivine crystal size distribution (CSD) profiles for different impact melt and basalt groups. (b) A-12 vitrophyric basalts, though similar in texture to the A-14 impact melts, have CSDs similar to the other members of their respective basalt suites. Individual olivine CSDs with the appropriate error bars are shown in Figs. 8 and 10.

its “cloudy” appearance. The relict portion (darker region) of the crystal has similar Co and Fo to olivine from 74275, but Ti/V ratio similar to the A-12 and A-14 basalts. Crystal #24 (,1486; Fig. 3d) has similar Fo and Mn to 74275, Co abundances on the high end of the A-14 basalts, but Y and Sc abundances akin to the OVs (Figs. 3a, 4, and 9). The complex similarities of these relict crystals with the basalts in this study suggest that they were likely inherited

from a basalt type compositionally intermediate to the A-14 high-Al basalts, the A-12 basalt suites, and the high-Ti A-17 basalt. A similarly rounded olivine crystal is found in 14321,1602 (Fig. 3b) and is chemically similar to A-14 basaltic olivines in Fo, Co and Ti/V, suggesting that it was likely inherited from an A-14 high-Al basalt (Figs. 3 and 5). This would indicate that the ,1602 OV crystallized after the high-Al basalts.

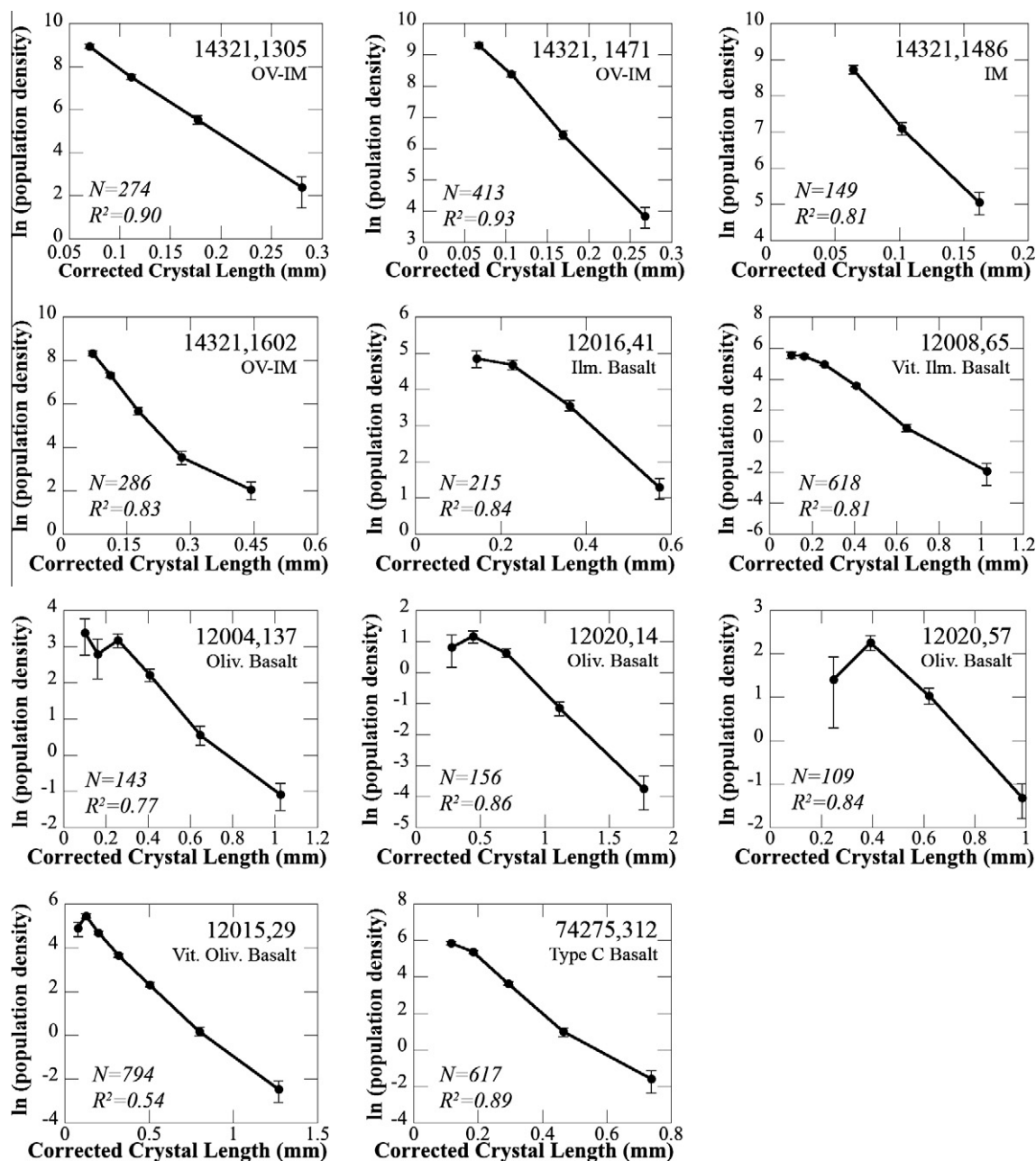


Fig. 8. Individual sample olivine CSDs from this study with associated error bars; the number of crystals used (N) and the corresponding correlation coefficient ( $R^2$  value) are also noted.

### 5.3. Apollo 12 basalts: olivine chemistry

The trace element compositions for olivines in the selected samples from the A-12 Pigeonite and Ilmenite basalt suites are nearly identical (Fig. 6, Table EA2) despite originating in isotopically distinct source regions (i.e. distinct  $^{87}\text{Sr}/^{86}\text{Sr}$  ratios; Nyquist et al., 1977). Although it may be possible to distinguish between the Olivine and Ilmenite basalt suites based on their olivine Ti/V ratios, olivine from the Pigeonite suite compositionally overlap those of the other basalt suites. With regards to other trace elements (Table EA2), the olivine

compositions of the selected Pigeonite suite members are similar to data from the other suites including those samples with vitrophyric textures. As such, although there are distinct differences between the whole rock chemistry of the A-12 basalt suites, it is difficult to confidently define the Pigeonite suite based solely on olivine compositions.

The wide range of olivine Sc (Fig. 6) and Co (Table EA2) abundances within the A-12 Olivine suite suggests that these selected samples may represent cumulates (cf. Walker et al., 1976; Neal et al., 1994b). In contrast, olivines in vitrophyric Olivine suite basalt 12015 do not

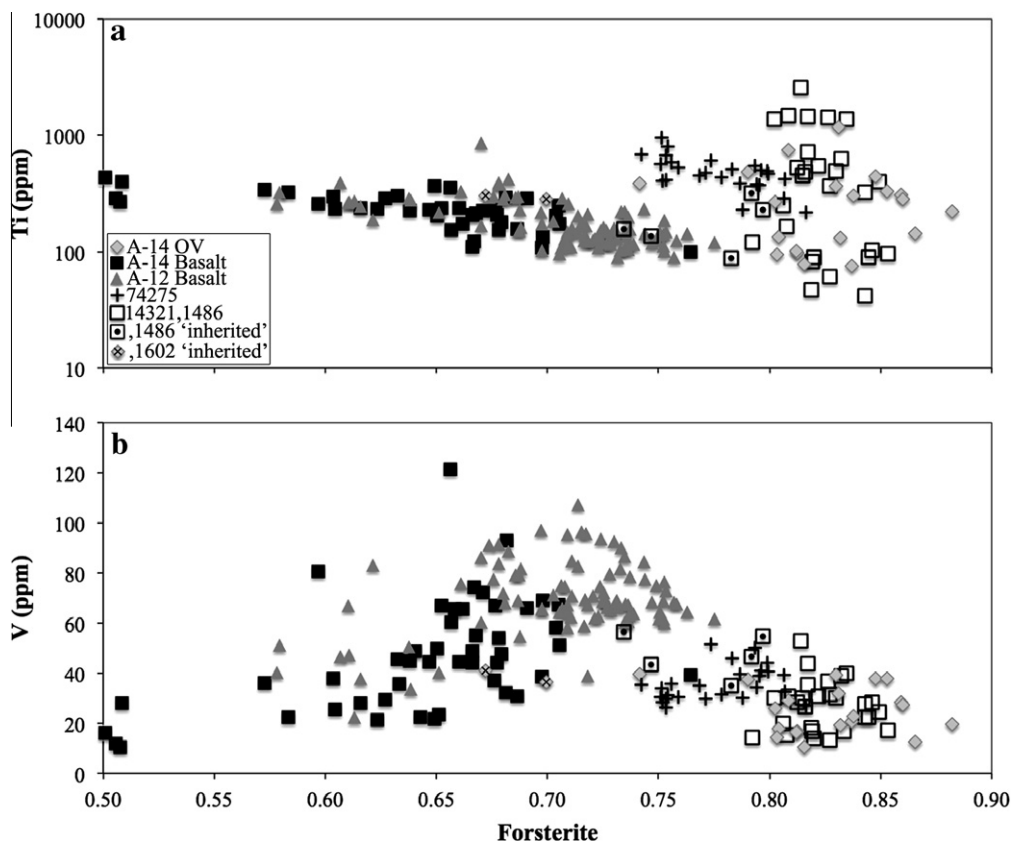


Fig. 9. Ti and V vs. Fo values for the olivine crystals in this study. Relict ('inherited') crystals from 14321,1486 and 14321,1602 are also indicated. Olivine crystals from Apollo basalts (A-12, A-14, and A-17) display different Fo–Ti (a) and Fo–V (b) relationships than the A-14 impact melt samples. This is also illustrated in the Ti/V ratio for these samples in Fig. 5.

exhibit a wide range of Sc contents. Thus, although members of the same suite, different crystallization histories likely explain the elemental variations between 12015 and the other Olivine suite samples in this study; textural evidence suggests that 12015 cooled more rapidly than 12004 and 12020 and did not undergo olivine accumulation. Although olivines from 12015 are distinct from those of the rest of the Olivine basalt suite, olivines from the vitrophyric Ilmenite suite basalt (12008) are compositionally indistinguishable from those of samples that comprise the rest of the suite (Fig. 6), suggesting that the Ilmenite suite basalts in this study did not experience olivine accumulation. Additionally, the olivine CSD of 12008 is subparallel to 12016 (Fig. 7b), suggesting that 12016 may have undergone relatively rapid cooling, though not to the same extent as its vitrophyric counterpart.

#### 5.4. Sample 74275,312

Olivines from A-17 sample 74275,312 are generally closer in composition to the A-14 impact melts than those from the various A-12 and A-14 basalt groups (e.g. Figs. 3a, 4b, 5, and 9a), particularly with regards to high Fo. This could be used as evidence of 74275 being an impact melt, but the corresponding CSD is similar to other pristine basalts in terms of its texture. Another, more likely,

explanation is that the A-14 impact melt target material may have included compositions similar to 74275,312 rather than an A-14 high-Al basalt. For 74275,312, the olivine compositions vary according to size with the smallest crystals having the lowest Fo as well as the highest Mn and Ti/V ratios; this sample is part of the high-Ti basalt suite, which explains, in part, the high Ti/V ratio. Conversely, the largest olivine phenocrysts have similar trace element compositions to olivine from the A-14 impact melts. This likely reflects prolonged olivine crystallization as this basalt cooled.

#### 5.5. Textural analysis

The 11 olivine textural analyses (Table 1; Figs. 7 and 8) for the A-12 and A-17 basalts and the A-14 impact melts complement earlier work that suggests plagioclase from A-14 impact melts may exhibit systematically different CSD shapes than those from the A-14 high-Al basalts (Hui et al., 2011). However, we note that the A-14 high-Al basalts did not contain a sufficient number of olivine (i.e. >100 crystals) to be able to perform a CSD analysis. Selected basalt groups from A-12 and A-17 are characterized by olivine CSD profiles that are distinct from those of the A-14 impact melts (Fig. 7). These distinctions are reflected by plagioclase CSDs by Neal et al. (2011), where

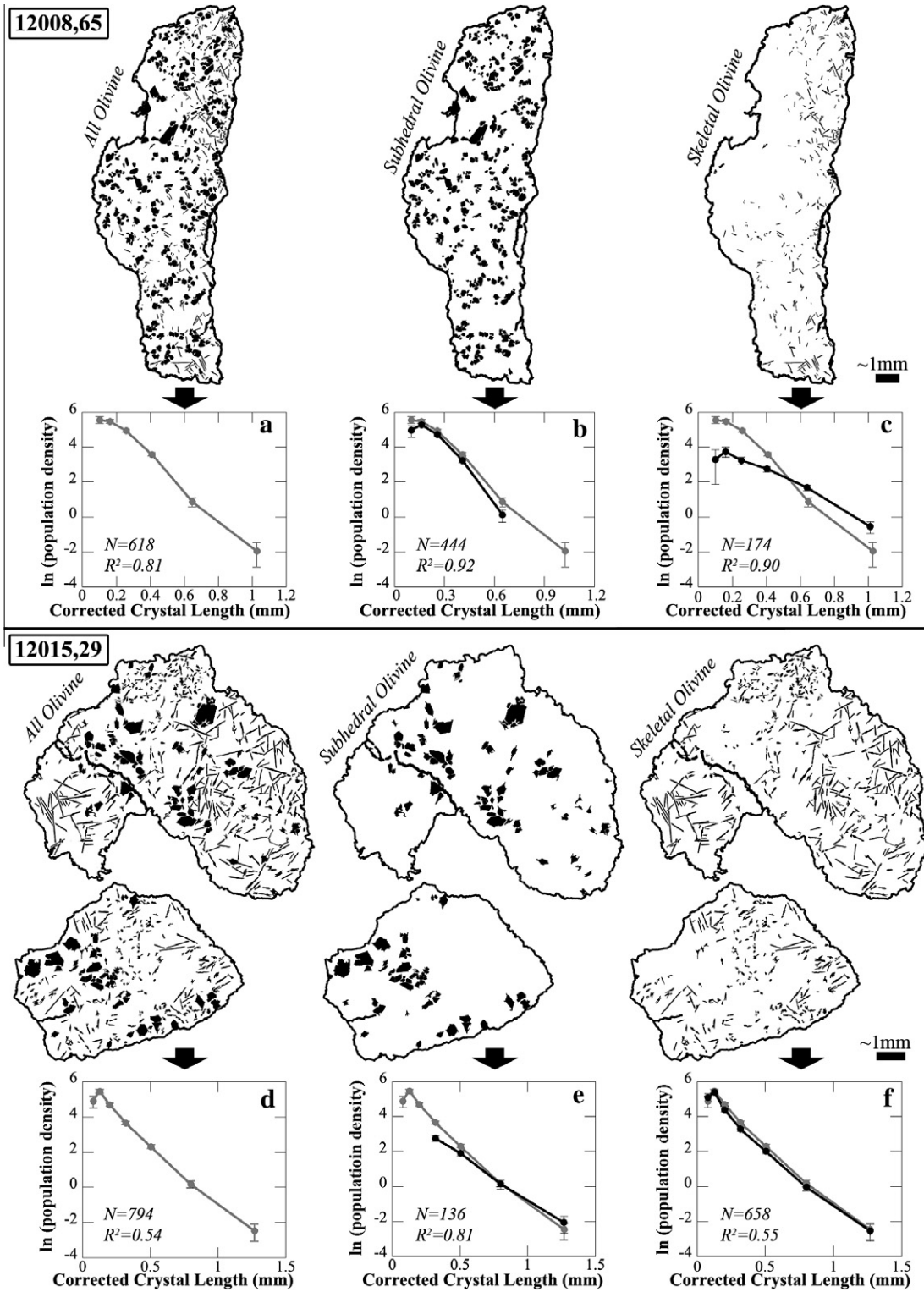


Fig. 10. Olivine CSDs for Apollo 12 basalts with vitrophyric textures; schematic diagrams for the thin-section of each sample’s crystal population are shown above the respective CSD plot. The total olivine crystal population CSDs are seen in (a and d) while the separated populations are exhibited in b-c and e-f for 12008 and 12015, respectively. Initial CSDs of the entire sample are shown in grey with subsequent analyses (b, c and e, f) in black for the purpose of comparison.

CSD slope differences indicate that the impact melt and basalt clasts from 14321 experienced markedly different

crystallizing conditions, thus providing further evidence that the high-Al basalts are not impact melts (cf. Snyder

et al., 2000; Snyder and Taylor, 2001). Using textural analyses of plagioclase in analogy, we can confirm our classification of 14321,1486 as an impact melt given that the olivine CSD is similar to those from the OV's (Fig. 7a). Furthermore, statistical models such as a simple Student *T*-test, show that the impact melt and basalt (A-12 and A-17) populations here have statistically unique CSD slopes as shown in Fig. 7.

The majority of CSD profiles are linear to sub-linear indicating a relatively constant cooling history and single crystal populations (Figs. 7 and 8). Several of the CSDs display a concave down profile at the smallest corrected crystal lengths (Fig. 8). This behavior is not a consequence of a change in crystallization history, but is a product of the resolution limit of the photomicrographs used to create the CSD. Although the samples contain olivine <0.05 mm in corrected crystal length, it is difficult to accurately represent these and an initial concave down pattern should be regarded as an artifact (“detection limit”) of the method. Additionally, as mentioned previously, any crystal <0.03 mm was eliminated from analysis on the basis of being projections of the crystal rather than accurate representations (Higgins, 2000).

Basalt clasts from 14321 contain relatively few olivine crystals making it difficult to construct a set of textural characteristics. In general, more than ~100 crystals are necessary to reliably determine the initial 3D crystal dimension (with an  $R^2 > 0.8$ ) using the *CSDslice* program. To combat this issue, olivine CSD analyses were conducted on a set of olivine-rich basalts from A-12 and A-17 to be able to compare and contrast olivine textures from pristine basalts to the A-14 impact melts. Most of the A-12 and A-17 basalt crystal dimensions fit the *CSDslice* model parameters well.

Textural analyses can be used to distinguish between the different A-12 basalt suites. The Ilmenite basalt suite displays olivine CSDs with steeper slopes than the Olivine suite basalts indicating a faster cooling rate; the vitrophyric varieties in each suite have similar slopes to each other (Fig. 7b). CSD analysis for the Pigeonite suite basalts examined in this study was not possible due to the small number of olivine crystals present. All of the A-12 CSDs have shallower slopes than the A-14 impact melts (Fig. 6) indicating a slower cooling history. Similarly, the olivine CSD for 74275,312 is clearly discernible from the impact melts, although the curved nature of the CSD is similar to that for 12008,65, suggesting either textural coarsening or at least two crystal populations with non-collinear straight CSDs (Higgins, 1996). The presence of two crystal populations is consistent with olivine accumulation (cf. Walker et al., 1976; Neal et al., 1994b) and is reflective of the presence of both microphenocrysts and phenocrysts as well as the major and trace element variations therein.

On the basis of their CSDs, the A-12 basalts with vitrophyric textures (12008 and 12015) are characterized by a unique cooling history. Taken as a whole, the crystal populations of 12015 define a less than ideal fit to the *CSDslice* model with  $R^2 = 0.54$  (Fig. 8). In an attempt to improve the CSD statistics for these two samples, the euhedral to subhedral olivine populations were manually separated from the skeletal olivine population (Fig. 10). The revised *CSDslice*

estimates of crystal habit for the 12008 olivine populations improve to  $R^2 = 0.90$ – $0.92$  (Fig. 10 b-c). Similarly with 12015, the separation of crystals enhances the model fit for the larger crystals ( $R^2 = 0.81$ , Fig. 10e), but only marginally improves the smaller crystal population ( $R^2 = 0.55$ , Fig. 10f), though Morgan and Jerram (2006) have noted that acicular crystal shapes are prone to low scores due to statistics of sectioning behavior. A-17 basalt 74275 has a similar sinuous CSD shape to 12008, but with a lack of clearly definable crystal shapes to use to separate populations, such as euhedral from skeletal, it is not possible at this time to conduct a similar operation. This shows that sometimes a single CSD is insufficient to represent the crystal populations of a sample and the inherent crystal cooling histories therein. For samples with low  $R^2$ -values, but sufficiently high number of crystals, manual manipulation may be required to obtain representative CSD profiles. The identification of multiple crystal populations can be particularly useful in selecting future geochemical analyses to ensure that the desired dataset (a) represents a single crystallization event or (2) encompasses all crystallization events for the sample.

## 6. CONCLUSIONS

This study clearly demonstrates that it is possible, using minimally destructive analytical techniques, to distinguish between Apollo sample types using olivine. Alternative methods such as whole-rock and highly-siderophile element analyses can also be used to clearly discriminate between impact melt and pristine mare basalts, but these methods are time-consuming and require relatively large amounts of priceless and irreplaceable sample material. On the basis of olivine chemistry from a variety of samples reported here, most of the different sample groups can be reliably identified using the following observations of olivine:

- (1) Impact melts have the highest forsterite values in the study.
- (2) The A-12 and A-14 basalts analyzed in this study have distinct trace element (e.g. Co, Mn, Y) abundances compared to those for the impact melts.
- (3) The A-12 basalts analyzed in this study have the highest Co, Sc, and V abundances of all the samples.
- (4) A subset of A-12 Olivine suite basalts is chemically distinct from selected A-12 Ilmenite suite basalts (e.g. Ti/V), but A-12 Pigeonite suite basalts compositionally overlap the Olivine and Ilmenite suites.
- (5) The olivine textural and trace element chemistries of the non-vitrophyric A-12 Olivine suite basalts indicate these samples experienced olivine accumulation.

This study has also shown that crystal size distributions, a completely non-destructive method, can be an effective tool in distinguishing between A-14 impact melts and basalts from A-12 and A-17. Olivine CSD slopes from A-14 impact melts are statistically steeper than the A-12 and A-17 basalts. Of interest, CSD slopes, which are dependent on the crystallization history of an individual sample, may differ depending on the basalt type as is noted among

the selected basalt samples from the A-12 suites examined here (Olivine and Ilmenite).

Olivine mineral chemistry and textural analyses can be used to differentiate between (1) impact melt and pristine mare basalt, (2) basalts from different landing sites, and (3) basalt groups from a single landing site. As proof of concept, the chemical and textural results from this study have clearly identified an olivine-rich impact melt that was previously characterized as a pristine A-14 high-Al basalt (14321,1486). The combined chemical and textural analysis approach adopted here can also identify distinct (inherited) olivine crystals within a single impact melt sample, and can infer the origin for these inherited crystals based on their similarity to olivine chemistry from A-14 or A-17 basalts.

#### ACKNOWLEDGMENTS

Many thanks are due to Paul Carpenter for his assistance with the use of the EPMA at Washington University in St. Louis and to Michael Hartney for statistical expertise. This work was funded in part by the University of Notre Dame Lilly Fellowship to A.L.F. (nee A.L.B.), NASA Cosmochemistry Grant NNX09AB92G and NASA (NLSI) USRA Subcontract #02173-05 to C.R.N. This manuscript was greatly improved by the careful, thorough, and constructive reviews of Katherine Joy and an anonymous reviewer.

#### APPENDIX A. SUPPLEMENTARY DATA

Supplementary data associated with this article can be found, in the online version, at <http://dx.doi.org/10.1016/j.gca.2012.12.032>.

#### REFERENCES

- Allen F. M., Bence A. E. and Grove T. L. (1979) Olivine vitrophyres in Apollo 14 breccia 14321: Samples of high-Mg component of the lunar highlands. In *10th Proc. Lunar Planet. Sci. Conf.* pp. 695–712.
- Boynnton W. V., Baedeker P. A., Chou C. -L., Robinson K. L. and Wasson J. T. (1975) Mixing and transport of lunar surface materials: Evidence obtained by the determination of lithophile, siderophile, and volatile elements. In *Sixth Proc. Lunar Planet. Sci. Conf.* pp. 2241–2259.
- Brett R., Butler, Jr., P., Meyer, Jr., C., Reid A. M., Takeda H. and Williams R. (1971) Apollo 12 igneous rocks 12004, 12008, 12009, and 12022: A mineralogical and petrological study. In *Second Proc. Lunar Sci. Conf.* pp. 301–317.
- Brown G. M., Peckett A., Emeleus C. H., Phillips R. and Pinsent R. H. (1975) Petrology and mineralogy of Apollo 17 mare basalts. In *Sixth Proc. Lunar Sci. Conf.* pp. 1–13.
- Cashman K. V. and Marsh B. D. (1988) Crystal size distribution (CSD) in rocks and the kinetics and dynamics of crystallization II: Makaopuhi lava lake. *Contrib. Mineral. Petrol.* **99**, 292–305.
- Compston W., Vernon M. J., Berry H. and Rudowski R. (1971) The age of the Fra Mauro Formation: A radiometric older limit. *Earth Planet. Sci. Lett.* **12**, 55–58.
- Compston W., Vernon M. J., Berry H., Rudowski R., Gray C. M. and Ware N. (1972) Apollo 14 mineral ages and the thermal history of the Fra Mauro formation. In *Third Proc. Lunar Sci. Conf.* pp. 1487–1501.
- Dasch E. J., Shih C.-Y., Bansal B. M., Wiesmann H. and Nyquist L. E. (1987) Isotopic analysis of basaltic fragments from lunar breccia 14321: Chronology and petrogenesis of pre-Imbrium mare volcanism. *Geochim. Cosmochim. Acta* **51**, 3241–3254.
- Dasch E. J., Shih C. -Y., Wiesmann H., Bansal B. M. and Nyquist L. E. (1991) Petrogenesis of A14 aluminous mare basalts: Results from 14072,48. In *22nd Lunar Planet. Sci. Conf.*
- Dickinson T., Taylor G. J. and Keil K. (1985) Apollo 14 aluminous mare basalts and their possible relationship to KREEP. *15th Proc. Lunar Planet. Sci. Conf. J. Geophys. Res.* **90**, C365–C374.
- Donaldson C. H. (1976) An experimental investigation of olivine morphology. *Contrib. Mineral. Petrol.* **57**, 187–213.
- Drever H. I., Johnston R., Butler P. and Gibb F. G. F. (1972) Some textures in Apollo 12 lunar igneous rocks and in terrestrial analogs. In *Third Proc. Lunar Planet. Sci. Conf.* pp. 171–184.
- Duncan A. R., Grieve R. A. F. and Weill D. F. (1975) The life and times of Big Bertha: Lunar breccia 14321. *Geochim. Cosmochim. Acta* **39**, 255–273.
- Dungan M. A. and Brown R. W. (1977) The petrology of the Apollo 12 ilmenite basalt suite. In *Eighth Proc. Lunar Sci. Conf.* pp. 1339–1381.
- Elardo S. M., McCubbin F. M. and Shearer, Jr., C. K. (2012) Chromite symplectites in Mg-suite troctolite 76535 as evidence for infiltration metasomatism of a lunar layered intrusion. *Geochim. Cosmochim. Acta* **87**, 154–177.
- French B. M., Walter L. S., Heinrich K. F. J., Loman, Jr., P. D., Doan, Jr., A. S. and Adler I. (1972) Composition of major and minor minerals in five Apollo crystalline rocks. NASA SP-306.
- Hagerty J. J., Shearer C. K. and Papike J. J. (2001) Trace element variability of the Apollo 14 high-Al basalts. A result of igneous process or sample size? In *32nd Lunar Planet. Sci. Conf.*
- Hagerty J. J., Shearer C. K. and Papike J. J. (2002) Using small basaltic lunar clasts to reconstruct the early magmatic history of the moon, *Wkshp. Moon Beyond*, abstract #3041.
- Hagerty J. J., Shearer C. K. and Papike J. J. (2003) Trace element characteristics of minerals in the Apollo 14 high-Al basalts: Implications for an igneous versus an impact origin. In *34th Lunar Planet. Sci. Conf.*
- Hagerty J. J., Shearer C. K. and Papike J. J. (2005) Petrogenesis of the Apollo 14 high-alumina basalts: Implications from ion microprobe analyses. *Geochim. Cosmochim. Acta* **69**, 5831–5845.
- Haskin L. A., Jacobs J. W., Brannon J. C. and Haskin M. A. (1977) Compositional dispersions in lunar and terrestrial basalts. In *Eighth Proc. Lunar Sci. Conf.* pp. 1731–1750.
- Higgins M. D. (1996) Crystal size distributions and other quantitative textural measurements in lavas and tuff from Egmont volcano (Mt. Taranaki) New Zealand. *Bull. Volcanol.* **58**, 194–204.
- Higgins M. D. (2000) Measurement of crystal size distributions. *Am. Mineral.* **85**, 1105–1116.
- Higgins M. D. and Chandrasekharan D. (2007) Nature of sub-volcanic magma chambers, Deccan Province, India: Evidence from quantitative textural analysis of plagioclase megacrysts in the giant plagioclase basalts. *J. Petrol.* **48**, 885–900.
- Hui H., Oshrin J. G. and Neal C. R. (2011) Investigation into the petrogenesis of Apollo 14 high-Al basaltic melts through crystal stratigraphy of plagioclase. *Geochim. Cosmochim. Acta* **75**, 6439–6460.
- Jochum K. P., Weis U., Still B., Kuzmin D., Yang Q., Raczek I., Jacob D. E., Stracke A., Birbaum K., Frick D. A., Günther D. and Enzweiler J. (2011) Determination of reference values for NIST SRM 610–617 glasses following ISO guidelines. *Geoanal. Res.* **35**, 397–429.

- Klein, Jr., C., Drake J. C. and Frondel C. (1971) Mineralogical, petrological, and chemical features of four Apollo 12 lunar microgabbros. In *Second Proc. Lunar Sci. Conf.* pp. 265–284.
- Klöck W. and Palme H. (1988) Partitioning of Siderophile and Chalcophile elements between sulfide, olivine, and glass in a naturally reduced basalt from Disko Island, Greenland. In *18th Proc. Lunar Planet. Sci. Conf.* pp. 471–483.
- Lindstrom M. M. and Haskin L. A. (1978) Causes of compositional variations within mare basalt suites. In *Ninth Proc. Lunar Planet. Sci. Conf.* pp. 465–486.
- Mark R. K., Cliff R. A., Lee-Hu C. and Wetherill G. W. (1973) Rb–Sr studies of lunar breccias and soils. In *Fourth Proc. Lunar Sci. Conf.* pp. 1785–1795.
- Mark R. K., Lee-Hu C. and Wetherill G. W. (1975) More on Rb–Sr in lunar breccia 14321. In *Sixth Proc. Lunar Planet. Sci. Conf.* pp. 1501–1507.
- Maxwell J. A. (1971) Chemical composition of Apollo 12 lunar samples 12004, 12033, 2051, 12052, and 12065. *Earth Planet. Sci. Lett.* **10**, 285–288.
- Morgan D. J. and Jerram D. A. (2006) On estimating crystal shape for crystal size distribution analysis. *J. Volcanol. Geotherm. Res.* **154**, 1–7.
- Neal C. R. (2001) Interior of the Moon: The presence of garnet in the primitive deep lunar mantle. *J. Geophys. Res.* **106**, 27865–27885.
- Neal C. R. and Kramer G. Y. (2006) The petrogenesis of the Apollo 14 high-Al mare basalts. *Am. Mineral.* **91**, 1521–1535.
- Neal C. R. and Taylor L. A. (1988) A re-evaluation of olivine vitrophyre petrogenesis. In *19th Lunar Planet. Sci. Conf.*
- Neal C. R. and Taylor L. A. (1989) Metasomatic products of the lunar magma ocean: The role of KREEP dissemination. *Geochim. Cosmochim. Acta* **53**, 529–541.
- Neal C. R., Taylor L. A., and Lindstrom M. M. (1988) Apollo 14 mare basalt petrogenesis: Assimilation of KREEP-like components by a fractionating magma. In *18th Proc. Lunar Planet. Sci. Conf.* pp. 139–153.
- Neal C. R., Taylor L. A. and Patchen A. D. (1989a) High alumina (HA) and very high potassium (VHK) basalt clasts from Apollo 14 Breccias, Part 1 – Mineralogy and petrology: Evidence of crystallization from evolving magmas. In *19th Proc. Lunar Planet. Sci. Conf.* pp. 137–145.
- Neal C. R., Taylor L. A., Schmitt R. A., Hughes S. S. and Lindstrom M. M. (1989b) High alumina (HA) and very high potassium (VHK) basalt clasts from Apollo 14 breccias, Part 2 – Whole rock geochemistry: Further evidence for combined assimilation and fractional crystallization within the lunar crust. In *19th Proc. Lunar Planet. Sci. Conf.* pp. 147–161.
- Neal C. R., Hacker M. D., Snyder G. A., Taylor L. A., Liu Y.-G. and Schmitt R. A. (1994a) Basalt generation at the Apollo 12 site, Part 1: New data, classification, and re-evaluation. *Meteoritics* **29**, 334–348.
- Neal C. R., Hacker M. D., Snyder G. A., Taylor L. A., Liu Y.-G. and Schmitt R. A. (1994b) Basalt generation at the Apollo 12 site, Part 2: Source heterogeneity, multiple melts, and crustal assimilation. *Meteoritics* **29**, 349–361.
- Neal C. R., Donohue P. H., Fagan A., Hui H. and O’Sullivan K. (2011) Using quantitative petrography to distinguish between pristine basalts and impact melts from the Moon. In *42nd Lunar Planet. Sci. Conf.*
- Nyquist L. E., Bansal B. M., Wooden J. L. and Wiesmann H. (1977) Sr-isotopic constraints on the petrogenesis of Apollo 12 mare basalts. In *Eighth Proc. Lunar Sci. Conf.* pp. 1383–1415.
- Papanastassiou D. A. and Wasserburg G. J. (1971) Lunar chronology and evolution from Rb–Sr studies of Apollo 11 and 12 samples. *Earth Planet. Sci. Lett.* **11**, 37–62.
- Papike J. J., Hodges F. N., Bence A. E., Cameron M. and Rhodes J. M. (1976) Mare basalts: crystal chemistry, mineralogy, and petrology. *Rev. Geophys. Space Phys.* **14**, 475–540.
- Pearce N. J. G., Perkins W. T., Westgate J. A., Gorton M. P., Jackson S. E., Neal C. R. and Chenery S. P. (1997) A compilation of new and published major and trace element data for NIST SRM 610 and NIST SRM 612 glass reference materials. *Geostand. Newslett.* **21**, 115–144.
- Rhodes J. M., Hubbard N. J., Wiesmann H., Rodgers K. V., Brannon J. C. and Bansal B. M. (1976) Chemistry, classification, and petrogenesis of Apollo 17 mare basalts. In *Seventh Proc. Lunar Sci. Conf.* pp. 1467–1489.
- Rhodes J. M., Blanchard D. P., Dungan M. A., Brannon J. C. and Rodgers K. V. (1977) Chemistry of Apollo 12 mare basalts: Magma types and fractionation processes. In *Eighth Proc. Lunar Sci. Conf.* pp. 1305–1338.
- Ringwood A. E. (1970) Petrogenesis of Apollo 11 basalts and implications for lunar origin. *J. Geophys. Res.* **75**, 6453–6479.
- Ridley, W. I. (1975) On high-alumina mare basalts. In *Sixth Proc. Lunar Sci. Conf.* pp. 131–145.
- Shearer C. K. and Papike J. J. (2005) Early crustal building processes on the Moon: Models for the petrogenesis of the magnesian suite. *Geochim. Cosmochim. Acta* **69**, 3445–3461.
- Schnetzler C. C. and Philpotts J. A. (1971) Alkali, alkaline earth, and rare-earth element concentrations in some Apollo 12 soils, rocks, and separated phases. In *Second Proc. Lunar Sci. Conf.* pp. 1101–1122.
- Shervais J. W., Taylor L. A. and Lindstrom M. M. (1984) Olivine vitrophyres – A non-pristine high-Mg component in lunar breccia 14321. In *15th Lunar Planet. Sci. Conf.*
- Shervais J. W., Taylor L. A. and Lindstrom M. M. (1985a) Apollo 14 mare basalts: Petrology and geochemistry of clasts from consortium breccia 14321. *15th Proc. Lunar Planet. Sci. Conf. J. Geophys. Res.* **90**(Suppl.), C375–C395.
- Shervais J. W., Taylor L. A. and Lindstrom M. M. (1985b) Olivine vitrophyres – A non-pristine high-MG component in lunar breccia 14321. In *16th Lunar Planet. Sci.* pp. 771–772.
- Shervais J. W., Taylor L. A., and Lindstrom M. M. (1988) Olivine vitrophyres: A nonpristine high-Mg component in lunar breccia 14321. In *18th Proc. Lunar Planet. Sci. Conf.* pp. 45–57.
- Snyder G. A. and Taylor L. A. (2001) Oldest mare basalts or impact melts? The role of differential melting of plagioclase in Apollo 14 high-Al basalts. *Met. Planet. Sci.* **36**(Suppl.), A194.
- Snyder G. A., Borg L. E., Nyquist L. E. and Taylor L. A. (2000) Chronology and isotopic constraints on lunar evolution. *Origin Earth Moon*, 361–395.
- Snyder G. A., Neal C. R., Taylor L. A. and Halliday A. N. (1997) Anatexis of lunar cumulate mantle in time and space: Clues from trace-element, strontium, and neodymium isotopic chemistry of parental Apollo 12 basalts. *Geochim. Cosmochim. Acta* **61**, 2731–2747.
- Taylor L. A., Shervais J. W., Hunter R. H., Shih C.-Y., Bansal B. M., Wooden J., Nyquist L. E. and Laul L. C. (1983) Pre-4.2 AE mare-basalt volcanism in the lunar highlands. *Earth Planet. Sci. Lett.* **56**, 33–47.
- Taylor S. R. (1982) *Planetary Science: A Lunar Perspective*. Lunar and Planetary Institute, Houston, TX, 481pp.
- Taylor S. R. and McLennan S. M. (1985) *The Continental Crust: Its Composition and Evolution*. Blackwell, Oxford, 312pp.
- Wakita H., Rey P., and Schmitt R. A. (1971) Abundances of the 14 rare-earth elements and 12 other trace elements in Apollo 12 samples: Five igneous and one breccia rocks and four soils. In *Second Proc. Lunar Planet. Sci. Conf.* pp. 1319–1329.
- Walker D., Longhi J., Kirkpatrick R. J., and Hays J.F. (1976) Differentiation of an Apollo 12 picrite magma. In *Seventh Proc. Lunar Planet. Sci. Conf.* pp. 1365–1389.

Wänke H., Wlotzka F., Baddenhausen H., Balacescu A., Spettel B., Teschke F., Jagoutz E., Kruse H., Quijano-Rico M. and Rieder R. (1971) Apollo 12 samples: Chemical composition and its relation to sample locations and exposure ages, the two component origin of the various soil samples and studies on lunar metallic particles. In *Second Proc. Lunar Science Conf.* pp. 1187–1208.

Wänke H., Palme H., Baddenhausen H., Dreibus G., Jagoutz E., Kruse H., Spettel B., Teschke F. and Thacker R. (1974)

Chemistry of Apollo 16 and 17 samples: bulk composition, late-stage accumulation and early differentiation of the Moon. In *Fifth Proc. Lunar Sci. Conf.* pp. 1307–1335.

Warren P. H., Kallemeyn G. W. and Kyte F. T. (1997) Siderophile element evidence indicates that Apollo 14 high-Al mare basalts are not impact melts. In *28th Lunar Planet. Sci. Conf.*

*Associate editor:* Alan D. Brandon

Sample & Type: Olivine Analysis:	14321,1305 OV								14321,1471 OV						14321,1486 Impact Melt		
	1	2	3a	3b	4	5	6a	6b	1	2	3	4	5	6	1	2	3
Trace Element Abundances (ppm)																	
Ca	1149	1246	1966	1515	1497	2487	2639	1506	1526	4321	2073	2786	2035	7768	N.A.	N.A.	N.A.
Sc	9.97	9.15	11.21	9.21	8.64	13.1	10.51	10.12	6.81	10.53	8.22	12.77	12.51	12.83	5.82	8.57	11.07
Ti	270	78	134	94	97	385	132	101	75	443	332	488	367	1168	492	544	1417
V	25.93	10.38	17.96	14.4	16.67	40	19.17	16.27	20.49	38	38	38	39	32	30	31	37
Cr	434	271	341	241	273	1147	391	249	293	1037	1060	762	818	569	624	662	813
Mn	1079	1232	1856	1418	1608	2001	1422	1502	1373	1298	1116	1900	1611	1544	1176	1363	1348
Co	23.79	48	39	29	27	31	38	27	26	29	23.68	14.66	20	19.03	29	26	34
Ni	30	37	55	45	22	20	26	9	16	15	23	<3	<3	<3	<37	<36	<36
Y	2.74	0.84	3.15	3.72	1.20	2.41	3.32	1.72	0.65	10.38	1.65	5.87	2.85	24.37	2.61	3.80	28
1 sigma Error																	
Ca	69	61	90	69	77	97	104	70	84	160	84	108	88	268	N.A.	N.A.	N.A.
Sc	0.55	0.44	0.56	0.45	0.48	0.57	0.51	0.49	0.48	0.57	0.43	0.6	0.59	0.6	0.79	0.81	0.92
Ti	11	4	6	4	5	14	5	4	4	16	12	18	14	41	28	29	53
V	0.96	0.39	0.66	0.53	0.63	1	0.7	0.6	0.8	1	1	1	1	1	1	1	1
Cr	18	11	14	11	12	49	18	12	12	35	35	26	28	20	23	24	29
Mn	34	39	59	45	51	63	45	48	44	41	35	60	51	49	38	43	43
Co	0.93	2	1	1	1	1	1	1	1	1	0.9	0.59	0.79	0.76	1	1	1
Ni	2	2	3	2	2	2	2	2	2	2	2	2	2	2	18	16	17
Y	0.18	0.07	0.17	0.18	0.10	0.13	0.17	0.11	0.08	0.45	0.10	0.27	0.16	0.91	0.18	0.22	1

\*OV=olivine vitrophyre; Apollo 14 Groups A, B, and C= designated group according to the classification of Neal and Kramer (2006)

\*\*Type C Apollo 17 basalt is classified as such according to Rhodes et al. (1976)

Sample & Type: Olivine Analysis:	14321,1486 Impact Melt																
	4	5	6	7	8	9	10	11	12	13	14a	14b	14c	15a	15b	16	17
Trace Element Abundances (ppm)																	
Ca	N.A.	N.A.	N.A.	N.A.	N.A.	N.A.	N.A.	N.A.	N.A.	N.A.	N.A.	N.A.	N.A.	N.A.	N.A.	N.A.	N.A.
Sc	8.46	6.77	4.4	6.93	4.68	7.26	6.43	10.08	6.62	6.14	7.89	9.47	8.34	9.12	9.46	8.29	6.42
Ti	403	89	<30	62	90	252	481	1382	166	97	87	156	136	1448	530	451	47
V	25	14.07	16.72	13.12	22.28	19.78	27	30	15.43	16.92	35	56	44	35	28	30	18.21
Cr	448	302	268	293	302	516	425	499	354	233	259	928	547	1164	644	698	266
Mn	1301	1394	1262	1440	1138	1541	1247	1650	1533	1100	1557	1944	1983	1448	1309	1317	1564
Co	31	44	38	42	34	27	35	28	33	40	19.00	36	45	31	23.85	21.38	31
Ni	<23	295	<22	<27	<26	<28	<13	<19	<15	30	<12	25	<16	<15	<13	<15	<15
Y	0.93	0.90	0.64	0.98	0.82	2.30	4.38	23.58	1.54	1.68	0.60	1.63	1.36	19.45	11.56	3.17	0.69
1 sigma Error																	
Ca	N.A.	N.A.	N.A.	N.A.	N.A.	N.A.	N.A.	N.A.	N.A.	N.A.	N.A.	N.A.	N.A.	N.A.	N.A.	N.A.	N.A.
Sc	0.87	0.96	0.76	0.85	0.69	0.75	0.5	0.69	0.51	0.57	0.49	0.54	0.67	0.64	0.57	0.53	0.54
Ti	26	24	18	22	20	34	40	108	20	20	15	19	16	130	51	46	15
V	1	0.75	0.74	0.66	0.87	0.8	1	1	0.66	0.76	1	2	2	1	1	1	0.77
Cr	18	15	13	15	15	23	17	20	15	12	11	36	20	46	26	29	13
Mn	42	45	40	46	36	49	40	52	49	35	49	62	63	46	42	42	50
Co	1	2	1	2	1	1	1	1	1	2	0.77	1	2	1	0.93	0.84	1
Ni	16	21	13	18	17	18	8	11	9	10	7	8	11	10	8	8	9
Y	0.11	0.13	0.09	0.11	0.09	0.15	0.22	0.89	0.11	0.14	0.07	0.11	0.11	0.78	0.48	0.17	0.08

Sample & Type: Olivine Analysis:	14321,1486 Impact Melt													14321,1602 OV			
	18a	18b	18c	19	20	21	22	23	24a	24b	25	26	27	1	2	3	4
Trace Element Abundances (ppm)																	
Ca	N.A.	N.A.	N.A.	N.A.	N.A.	N.A.	N.A.	N.A.	N.A.	N.A.	N.A.	N.A.	N.A.	2691	7092	1905	2666
Sc	12.69	10.07	5.09	6.03	3.64	5.16	9.85	7.59	6.61	7.71	9.94	5.99	10.7	16	21	14.52	20
Ti	2582	1480	121	82	41	104	626	322	231	319	1376	365	728	306	747	221	280
V	53	31	14.43	16.87	22.31	28	39	27.79	55	47	40	32	44	28	29	19.65	27
Cr	1712	560	238	274	342	410	726	711	1453	1319	794	739	1320	832	686	404	469
Mn	1464	1154	1619	1324	1231	1402	1526	1123	1688	1688	1626	1386	1549	1071	1412	776	1245
Co	32	24	31	36	42	51	36	25.18	84	84	41	25.67	31	29	54	23.02	31
Ni	<20	<15	<16	<16	<18	<18	<20	<14	46	202	75	<15	<15	79	362	30	28
Y	46	28	0.53	1.11	0.70	1.27	3.87	2.25	2.92	2.86	33	2.56	10.66	4.27	21.21	1.72	4.27
1 sigma Error																	
Ca	N.A.	N.A.	N.A.	N.A.	N.A.	N.A.	N.A.	N.A.	N.A.	N.A.	N.A.	N.A.	N.A.	212	266	96	168
Sc	0.91	0.71	0.77	0.55	0.56	0.66	0.7	0.52	0.56	0.58	0.85	0.56	0.64	2	1	0.74	1
Ti	276	163	26	17	16	22	85	46	36	17	50	18	28	15	26	8	12
V	2	1	0.75	0.67	0.85	1	1	0.98	2	2	1	1	1	1	1	0.72	1
Cr	82	29	16	16	19	24	41	42	88	44	29	26	44	31	23	14	18
Mn	47	37	52	42	39	45	48	36	54	54	52	44	49	34	45	25	40
Co	1	1	1	1	2	2	1	0.97	3	3	2	0.99	1	1	2	0.81	1
Ni	15	12	15	10	11	13	12	8	10	13	15	10	9	5	12	2	3
Y	2	1	0.11	0.09	0.08	0.12	0.19	0.13	0.16	0.15	1	0.15	0.40	0.36	0.79	0.11	0.29

Sample & Type: Olivine Analysis:	14321,1602 OV				14321,1246 Group A						14321,1480 Group A				14321,1611 Group A		
	5a	5b	6	7	1a	1b	2	3a	3b	4	1	2	3	4	1	2	3
Trace Element Abundances (ppm)																	
Ca	3274	3256	2584	3026	4185	2909	3225	2801	2988	2088	N.A.	N.A.	N.A.	N.A.	1905	2673	2430
Sc	23	21.06	17.44	12.71	23	20.68	22.15	18.66	18.55	11.49	20	22	<6	17	22	20	18.68
Ti	281	301	143	305	246	285	248	204	173	99	287	365	294	344	324	437	237
V	37	41	12.39	22.8	67	66	67	58	51	39	29	22	32	36	22.29	15.91	45
Cr	532	940	395	668	1974	1705	1990	1207	1671	1359	382	459	708	673	502	301	1033
Mn	2596	2516	1194	1062	2537	2578	2634	2357	2299	1970	2412	2389	2100	2659	2626	3237	2029
Co	65	38	53	32	58	69	73	68	63	78	52	53	68	57	52	65	48
Ni	59	22	128	85	24	35	51	45	38	141	<15986	<924	<449	<330	30	18	18
Y	1.27	2.29	4.05	4.47	1.39	0.62	0.31	0.23	0.31	0.08	<0.60	1.47	<0.67	1.74	0.40	5.33	0.61
1 sigma Error																	
Ca	142	139	134	128	159	122	131	121	123	97	N.A.	N.A.	N.A.	N.A.	122	126	110
Sc	1	0.94	0.95	0.64	1	0.94	0.98	0.89	0.86	0.64	3	3	3	3	1	1	0.88
Ti	10	11	6	11	9	10	9	8	7	5	48	61	57	69	13	16	9
V	1	1	0.51	0.84	2	2	2	2	2	1	1	1	2	2	0.82	0.59	2
Cr	18	31	14	22	63	55	64	39	54	50	27	32	47	47	18	11	33
Mn	82	80	38	34	80	82	83	75	73	62	77	77	67	85	83	103	64
Co	2	1	2	1	2	2	2	2	2	3	4	4	4	4	2	2	2
Ni	3	2	5	3	2	2	2	2	2	6	1596515	4407	1500	217	2	2	2
Y	0.09	0.12	0.22	0.19	0.10	0.06	0.04	0.04	0.04	0.03	0.30	0.34	0.35	0.34	0.07	0.26	0.07

Sample & Type: Olivine Analysis:	14321,1611 Group A			14321,1376 Group B						14321,1482 Group B					
	4	5	6	1	2a	2b	3a	3b	3c	1a	1b	2a	2b	3	4
Trace Element Abundances (ppm)															
Ca	3047	2296	2520	N.A.	N.A.	N.A.	N.A.	N.A.	N.A.	N.A.	N.A.	N.A.	N.A.	N.A.	N.A.
Sc	17.85	21	25	<29	<23	<27	<25	<22	<22	14	15	12	14	22	13
Ti	400	270	289	<302	<230	<262	<267	<225	<219	111	156	108	178	235	233
V	27.82	10.3	11.77	93	23	65	22	49	36	44	31	38	48	21	26
Cr	1485	170	140	3699	207	2159	228	1143	766	1347	389	831	1358	142	252
Mn	2998	3202	3245	2585	2341	2713	2740	2541	2688	2285	2228	2216	2523	2658	2460
Co	63	61	61	<33	<27	<32	<30	49	<26	62	64	73	73	29	55
Ni	36	30	30	<674	<513	<621	<568	<531	<492	<118	<121	<128	<154	<128	<142
Y	5.63	3.75	3.20	<4	<2.48	<4	<2.96	<3	<2.70	0.70	0.82	<0.61	1.22	0.92	1.64
1 sigma Error															
Ca	127	113	115	N.A.	N.A.	N.A.	N.A.	N.A.	N.A.	N.A.	N.A.	N.A.	N.A.	N.A.	N.A.
Sc	0.87	1	1	9	7	9	8	7	7	2	2	2	3	2	3
Ti	15	10	11	96	73	86	87	73	71	25	27	26	34	36	38
V	0.97	0.41	0.45	4	2	3	2	2	2	2	1	2	2	1	1
Cr	48	7	6	193	40	129	49	81	63	113	37	79	137	20	33
Mn	95	101	103	83	75	87	88	81	86	73	71	71	81	85	79
Co	2	2	2	11	8	10	9	9	8	4	4	4	5	3	4
Ni	2	2	2	663	480	686	597	641	690	50	54	65	72	115	129
Y	0.27	0.21	0.18	1	0.79	1	0.94	1	0.87	0.29	0.29	0.28	0.33	0.29	0.35

Sample & Type: Olivine Analysis:	14321,1483 Group B					14321,1612 Group B						14321,9057 Group C			14321,9080 Group C		
	1a	1b	1c	2	3	1	2	3	4	5	6	1	2	3	1	2	3
Trace Element Abundances (ppm)																	
Ca	361	1764	2471	3755	4539	2793	2602	2973	2379	2490	2098	N.A.	N.A.	N.A.	N.A.	N.A.	N.A.
Sc	27	36	37	36	37	22.71	21.33	22.25	22.43	21.84	24.09	13.79	9.71	12.09	10.46	9.55	13.72
Ti	152	206	208	225	354	229	229	260	296	227	237	304	204	174	238	133	154
V	54	49	44	72	121	37	45	81	38	45	27.86	45	50	66	67	69	60
Cr	1411	912	674	1850	3581	1158	946	2888	915	1140	236	898	1327	1826	1638	1827	1495
Mn	1893	2442	2375	2410	2473	2723	2522	2905	3003	2700	2665	2517	2471	2656	2711	2432	2339
Co	56	60	63	72	71	76	45	52	64	66	55	69	71	86	80	82	65
Ni	39	40	38	50	37	40	23	15	12	22	4	<15	<12	54	<15	<15	<15
Y	0.73	1.33	1.02	2.14	1.72	1.50	0.89	3.59	5.00	1.53	0.97	1.50	1.65	1.31	0.40	0.23	0.54
1 sigma Error																	
Ca	126	143	156	170	178	116	102	116	97	103	90	N.A.	N.A.	N.A.	N.A.	N.A.	N.A.
Sc	2	2	2	2	2	0.97	0.87	0.91	0.91	0.90	0.96	0.72	0.65	0.77	0.71	0.66	0.79
Ti	6	8	9	9	13	9	8	9	10	8	9	12	8	8	11	7	8
V	2	2	2	2	4	1	1	3	1	1	0.93	2	2	2	2	2	2
Cr	45	30	22	59	114	37	30	91	29	36	8	31	47	67	58	65	54
Mn	60	77	75	76	78	86	80	92	95	85	84	80	78	84	86	77	74
Co	2	2	2	2	2	2	1	2	2	2	2	2	2	3	3	3	2
Ni	2	2	2	2	2	2	1	1	1	2	1	5	7	8	10	10	11
Y	0.07	0.10	0.10	0.13	0.11	0.10	0.06	0.16	0.21	0.09	0.07	0.11	0.11	0.10	0.07	0.06	0.07

Sample & Type: Olivine Analysis:	14321,9080 Group C		12008,65 Ilm Basalt										12015,29 Oliv Basalt				
	4	5	1a	1b	2	3	4	5a	5b	5c	6	7	1	2a	2b	3a	3b
Trace Element Abundances (ppm)																	
Ca	N.A.	N.A.	N.A.	N.A.	N.A.	N.A.	N.A.	N.A.	N.A.	N.A.	N.A.	N.A.	N.A.	N.A.	N.A.	N.A.	N.A.
Sc	11.26	11.91	10.2	8.83	8.96	13.31	13.33	10.21	12.9	9.68	11.19	10.03	11	12	5	5	10
Ti	215	122	296	259	287	424	392	300	382	284	295	309	160	222	117	102	232
V	55	75	69	64	66	89	84	77	92	72	79	68	93	87	64	82	85
Cr	1319	2013	2044	2033	2290	2503	2397	2125	2452	1981	2209	2007	3005	2958	2317	2681	2973
Mn	2238	2409	2238	2037	2091	2649	2711	2378	2680	2192	2440	2192	2117	2125	1627	1946	2118
Co	66	75	108	109	113	131	131	116	131	109	116	109	121	108	95	110	120
Ni	<14	<15	103	134	143	116	68	96	113	114	103	90	179	123	182	<117	138
Y	0.93	0.39	0.19	0.21	0.19	0.61	0.37	0.34	0.37	0.26	0.24	0.40	<0.54	<0.66	<0.42	0.58	<0.71
1 sigma Error																	
Ca	N.A.	N.A.	N.A.	N.A.	N.A.	N.A.	N.A.	N.A.	N.A.	N.A.	N.A.	N.A.	N.A.	N.A.	N.A.	N.A.	N.A.
Sc	0.69	0.73	0.64	0.61	0.62	0.81	0.84	0.78	0.84	0.72	0.9	0.74	2	2	2	2	3
Ti	10	7	12	11	12	17	17	14	17	13	15	15	23	29	21	26	32
V	2	3	2	2	2	3	3	3	3	3	3	3	3	3	2	3	3
Cr	48	75	73	73	83	91	89	80	93	77	88	80	207	209	167	199	228
Mn	71	76	71	65	66	84	86	75	85	70	78	70	68	68	52	63	68
Co	2	3	4	4	4	5	5	4	5	4	4	4	5	5	4	5	6
Ni	9	10	12	13	14	15	14	14	15	14	17	14	53	61	48	59	67
Y	0.08	0.06	0.06	0.06	0.06	0.08	0.07	0.07	0.08	0.06	0.08	0.07	0.24	0.30	0.24	0.31	0.36

Sample & Type: Olivine Analysis:	12015,29 Oliv Basalt						12005,44 Ilm. Basalt							
	4	5a	5b	5c	6	7	1a	1b	2a	2b	3a	3b	4	5b
Trace Element Abundances (ppm)														
Ca	N.A.	N.A.	N.A.	N.A.	N.A.	N.A.	N.A.	N.A.	N.A.	N.A.	N.A.	N.A.	N.A.	N.A.
Sc	14	4	15	12	12	11	7.81	10.81	10.66	9.66	7.74	8.42	8.24	9.55
Ti	203	157	153	145	223	148	212	288	331	278	216	247	228	273
V	108	85	94	83	90	95	39	51	76	34	40	38	55	22.33
Cr	2927	2481	2901	2372	3214	2620	683	943	2073	806	859	718	1231	530
Mn	2289	1954	2179	1897	2282	2128	1936	2943	2401	2401	2478	2633	2246	2401
Co	121	103	120	95	133	116	103	123	108	105	103	98	109	103
Ni	152	166	187	210	<136	<109	95	43	40	<17	23	<18	130	<15
Y	0.61	<0.60	<0.65	<0.57	<0.66	<0.50	0.31	1.83	0.77	1.94	1.50	2.52	0.17	1.69
1 sigma Error														
Ca	N.A.	N.A.	N.A.	N.A.	N.A.	N.A.	N.A.	N.A.	N.A.	N.A.	N.A.	N.A.	N.A.	N.A.
Sc	2	2	3	2	3	2	0.62	0.77	0.69	0.66	0.64	0.65	0.63	0.67
Ti	30	26	29	25	34	28	10	13	14	12	10	11	11	13
V	4	3	3	3	4	4	1	2	3	1	1	1	2	0.85
Cr	233	205	249	212	300	255	30	41	90	36	40	34	59	29
Mn	73	63	70	61	73	68	61	93	76	76	79	83	71	76
Co	6	5	6	5	7	6	4	4	4	4	4	3	4	4
Ni	64	59	67	59	70	60	11	12	11	10	10	10	13	10
Y	0.32	0.27	0.33	0.24	0.34	0.25	0.06	0.12	0.08	0.12	0.11	0.14	0.05	0.12

Sample & Type: Olivine Analysis:	12016,41 Ilm. Basalt				12004,137 Oliv. Basalt												
	1a	1b	2a	2b	1	2	3	4a	4b	5	6a	6b	7a	7b	8a	8b	9a
Trace Element Abundances (ppm)																	
Ca	1718	2792	1480	1199	1070	1390	1483	1324	1079	1231	1010	1010	913	1342	1075	1224	843
Sc	11.02	12.05	9.77	9.2	26	30	27	22	24	23	20	22	23	32	25	22	19
Ti	265	397	267	257	116	168	163	124	90	129	102	119	110	143	108	121	97
V	67	47	47	40	65	96	82	59	69	75	66	68	63	78	75	69	64
Cr	1969	859	1330	898	2171	2948	1837	1447	2451	2008	2098	2948	1934	2487	1803	2108	2007
Mn	2575	2743	2429	2744	1979	2473	2451	1908	1909	2101	1914	1783	1903	2536	2221	2112	2182
Co	101	102	94	103	103	123	103	92	104	103	89	93	95	137	109	103	93
Ni	103	55	74	55	202	216	100	167	218	186	170	197	183	287	146	184	163
Y	0.33	1.18	0.26	1.32	<0.07	0.22	0.35	0.11	0.11	0.24	<0.07	0.19	0.08	0.23	0.14	0.18	0.14
1 sigma Error																	
Ca	106	139	100	100	75	93	89	102	129	77	100	75	61	87	106	112	106
Sc	0.86	0.89	0.79	0.81	1	2	1	1	2	1	1	1	1	2	2	1	1
Ti	10	14	10	9	5	7	7	6	6	5	5	5	4	6	6	6	6
V	2	2	2	1	2	3	3	2	2	2	2	2	2	3	3	2	2
Cr	64	29	43	30	68	92	58	46	78	63	66	92	61	78	57	67	64
Mn	81	87	77	87	63	78	78	60	61	67	61	56	60	80	70	67	69
Co	3	3	3	3	3	4	3	3	3	3	3	3	3	4	4	3	3
Ni	5	4	4	4	7	7	3	6	8	6	6	6	6	9	5	6	6
Y	0.06	0.08	0.05	0.09	0.05	0.07	0.06	0.06	0.10	0.05	0.07	0.06	0.04	0.07	0.08	0.08	0.08

Sample & Type: Olivine Analysis:	12004,137 Oliv. Basalt			12020,14 Oliv. Basalt													
	9b	9c		1a	1b	1c	2a	2b	2c	3a	3b	4	5a	5b	6	7	8a
Trace Element Abundances (ppm)																	
Ca	950	1109		1464	1333	1695	1358	1393	1429	1075	971	959	927	823	1260	1161	1148
Sc	18	22		42	55	61	57	60	47	48	47	38	42	38	38	35	41
Ti	90	131		151	160	201	139	149	166	126	113	123	116	106	153	140	132
V	66	80		79	71	67	70	69	60	71	62	67	63	60	69	67	75
Cr	2217	3023		2141	2066	2281	2109	2244	1626	2338	2255	2124	2138	2012	2216	1976	2466
Mn	2136	1904		2385	2085	2084	2200	2150	2323	2043	1900	1976	1911	1791	2005	2084	2310
Co	108	95		103	95	104	101	104	112	103	100	99	98	91	98	95	113
Ni	204	196		148	181	234	204	219	125	228	234	206	209	195	193	170	223
Y	0.12	0.32		0.15	<0.15	0.33	0.22	<0.14	0.26	<0.12	0.13	<0.11	<0.12	0.15	<0.10	<0.11	0.20
1 sigma Error																	
Ca	152	106		83	81	94	86	86	82	71	65	64	62	60	70	67	77
Sc	2	1		2	3	3	3	3	2	2	2	2	2	2	2	2	2
Ti	7	7		6	6	8	6	6	6	5	5	5	5	4	6	6	5
V	2	3		3	3	3	3	3	2	3	3	3	3	3	2	2	2
Cr	72	95		67	65	71	66	70	51	73	71	67	67	63	73	65	82
Mn	68	60		75	66	66	70	68	74	65	60	63	60	57	63	66	73
Co	4	3		3	3	3	3	3	4	3	3	3	3	3	3	3	4
Ni	8	7		5	6	8	7	7	4	8	8	7	7	7	6	6	7
Y	0.12	0.09		0.06	0.08	0.09	0.09	0.08	0.08	0.07	0.07	0.06	0.07	0.06	0.05	0.06	0.07

Sample & Type: Olivine Analysis:	12020,14 Oliv. Basalt							12020,57 Oliv. Basalt									
	8b	9a	9b	10a	10b	11a	11b	1	2	3	4	5a	5b	6a	6b	7a	7b
Trace Element Abundances (ppm)																	
Ca	924	1034	1134	936	1044	844	1042	1107	1299	1068	1055	1380	1052	1233	1146	1403	1676
Sc	32	41	37	32	37	30	32	25	30	34	35	35	26	32	32	34	36
Ti	118	125	145	101	109	117	139	129	130	147	182	156	137	140	120	151	185
V	66	68	64	60	63	58	62	62	69	68	71	78	61	69	62	69	77
Cr	2115	2501	2432	2190	2336	1732	2282	2048	2299	2248	2180	2762	1879	2274	2009	2444	2883
Mn	2073	2042	2011	1802	2035	2069	1876	1804	2015	2010	1987	2202	1852	1915	1732	2141	2228
Co	102	112	105	99	106	97	105	94	110	111	103	125	91	108	104	116	129
Ni	196	256	231	219	226	147	174	197	235	247	216	280	174	241	246	252	298
Y	<0.10	0.24	0.26	0.24	0.13	<0.10	0.31	0.17	0.13	0.18	0.19	0.20	0.15	0.18	0.22	0.16	0.27
1 sigma Error																	
Ca	66	76	76	64	68	60	73	57	68	63	60	73	56	66	63	72	84
Sc	2	2	2	2	2	1	2	1	1	2	2	2	1	1	1	2	2
Ti	5	5	6	4	5	5	6	5	5	6	7	6	5	5	5	6	7
V	2	2	2	2	2	2	2	2	2	2	2	3	2	2	2	2	2
Cr	70	84	82	74	80	60	80	64	72	70	68	86	59	71	63	76	90
Mn	66	65	64	57	64	65	59	57	64	64	63	70	59	61	55	68	70
Co	3	4	3	3	3	3	3	3	3	4	3	4	3	3	3	4	4
Ni	6	8	8	7	7	5	6	6	8	8	7	9	6	8	8	8	10
Y	0.06	0.07	0.07	0.06	0.06	0.05	0.07	0.05	0.05	0.05	0.05	0.06	0.04	0.05	0.05	0.06	0.06

Sample & Type: Olivine Analysis:	12020,57 Oliv. Basalt					12019,5 Pig. Basalt			12052,345 Pig. Basalt		12065,109 Pig. Basalt	
	8	9a	9b	10a	10b	1a	1b	1c	1a	1b	1a	1b
Trace Element Abundances (ppm)												
Ca	1395	1319	1477	775	1080	1488	1925	2180	2441	1702	1558	1443
Sc	31	32	33	27	32	11.53	9.68	10.69	10.97	9.86	9.21	8.87
Ti	161	143	147	105	126	177	865	292	324	189	219	174
V	72	64	73	61	75	97	86	91	51	83	97	65
Cr	2429	2299	2561	2088	2813	2970	2088	2138	913	1803	2532	1732
Mn	2163	1901	2094	1768	2143	2424	2197	2457	3196	2454	2602	2095
Co	114	112	122	103	132	136	102	111	86	95	115	81
Ni	242	261	280	225	306	245	37	46	<5	20	91	348
Y	0.35	0.21	<0.12	<0.09	0.35	0.22	0.37	0.35	1.12	0.20	0.37	0.17
1 sigma Error												
Ca	72	68	76	52	67	112	107	120	141	109	120	84
Sc	1	1	2	1	2	0.79	0.64	0.69	0.7	0.64	0.59	0.43
Ti	6	5	6	4	5	7	29	11	12	7	9	6
V	2	2	2	2	2	3	3	3	2	3	3	2
Cr	76	72	80	65	88	94	66	68	30	57	80	54
Mn	68	60	66	56	68	77	70	78	101	78	82	66
Co	4	4	4	3	4	4	3	4	3	3	4	3
Ni	8	8	9	7	10	9	3	4	3	3	8	13
Y	0.05	0.05	0.05	0.04	0.06	0.06	0.06	0.06	0.10	0.06	0.09	0.05

Sample & Type: Olivine Analysis:	74275,312 Type C Basalt																
	1a	1b	1c	1d	1e	2a	2b	2c	3	4	5a	5b	6a	6b	7a	7b	7c
Trace Element Abundances (ppm)																	
Ca	1460	1119	1177	939	1283	980	1029	1111	2677	2305	1051	1063	1145	1446	1482	1486	1208
Sc	13.39	9.97	12.25	8.16	11.74	10.85	10.49	10.44	14.98	11.19	9.98	7.73	9.4	12.83	10.75	10.2	10.04
Ti	612	498	547	377	509	449	468	491	962	678	422	219	230	480	417	286	440
V	52	41	50	34	46	35	41	44	34	30	33	26.9	30	30	26.36	39	31
Cr	1891	1740	1991	1377	1857	1384	1711	1797	1511	1294	1202	991	1303	1325	1239	1489	1360
Mn	2200	1624	1981	1392	1866	1694	1617	1685	2158	2039	1625	1358	1741	1827	1809	1813	1750
Co	57	48	57	39	52	50	47	52	50	47	46	40	47	44	43	55	43
Ni	<10	<9	<10	<7	<9	<8	<8	<8	<9	<8	42	34	22	<8	<8	69	<8
Y	0.31	0.30	0.33	0.26	0.48	0.31	0.25	0.38	0.98	1.51	0.18	0.28	0.32	0.46	0.31	0.20	0.36
1 sigma Error																	
Ca	113	95	104	79	99	81	90	96	147	130	92	85	94	98	95	112	92
Sc	0.76	0.61	0.72	0.51	0.67	0.59	0.61	0.63	0.78	0.64	0.61	0.51	0.58	0.67	0.59	0.66	0.59
Ti	23	19	21	15	20	18	19	20	38	28	18	10	9	18	16	12	17
V	2	1	2	1	2	1	1	2	1	1	1	0.96	1	1	0.89	1	1
Cr	81	75	87	61	85	65	82	89	77	68	66	56	55	56	53	64	59
Mn	70	51	63	44	59	54	51	53	68	65	51	43	55	58	57	57	55
Co	2	2	2	1	2	2	2	2	2	2	2	1	2	2	1	2	1
Ni	6	5	5	4	4	4	4	4	5	6	7	6	5	4	4	8	4
Y	0.08	0.07	0.07	0.05	0.07	0.05	0.06	0.07	0.09	0.11	0.06	0.05	0.06	0.06	0.06	0.06	0.06

Sample & Type: Olivine Analysis:	74275,312 Type C Basalt							
	8a	8b	9a	9b	9c	10	11	12

Trace Element Abundances (ppm)

Ca	1371	1721	1107	1011	1069	2191	1699	1394
Sc	11.07	12.37	9.58	8.23	8.8	13.79	13.47	13.58
Ti	527	582	405	371	386	805	568	687
V	31	36	28.37	39	39	31	30	35
Cr	1385	1511	1428	1671	1738	1412	1422	1528
Mn	1791	1872	1994	1571	1719	2144	2202	2099
Co	43	43	51	46	48	49	48	48
Ni	<7	<7	<9	<7	<8	<8	<8	<9
Y	2.14	0.89	0.34	0.26	0.36	0.85	0.55	0.47

1 sigma Error

Ca	105	114	96	85	90	137	115	106
Sc	0.64	0.68	0.62	0.52	0.56	0.75	0.73	0.73
Ti	20	23	16	15	16	32	23	28
V	1	1	0.99	1	1	1	1	1
Cr	61	68	66	78	83	69	72	79
Mn	57	59	63	50	54	68	70	66
Co	1	2	2	2	2	2	2	2
Ni	4	4	5	4	4	5	5	5
Y	0.14	0.09	0.07	0.05	0.06	0.09	0.07	0.07